2006-06

High-power amplifier free electron lasers

Voughs, Tyrone Y.

Monterey California. Naval Postgraduate School

NAVAL POSTGRADUATE SCHOOL

MONTEREY, CALIFORNIA

THESIS

HIGH-POWER AMPLIFIER FREE ELECTRON LASERS

by

Tyrone Y. Voughs

June 2006

Thesis Advisor:	William B. Colson
Co-Advisor:	Robert L. Armstead

Approved for public release; distribution is unlimited

THIS PAGE INTENTIONALLY LEFT BLANK

REPORT DOCUMENTATION PAGE		Form Approved OMB No. 0704-0188

1. AGENCY USE ONLY *(Leave blank)*	2. REPORT DATE June/2006	3. REPORT TYPE AND DATES COVERED Master's Thesis

4. TITLE AND SUBTITLE High-Power Amplifier Free Electron Lasers	5. FUNDING NUMBERS
6. AUTHOR(S) LT Tyrone Y. Voughs	
7. PERFORMING ORGANIZATION NAME(S) AND ADDRESS(ES) Naval Postgraduate School Monterey, CA 93943-5000	8. PERFORMING ORGANIZATION REPORT NUMBER
9. SPONSORING /MONITORING AGENCY NAME(S) AND ADDRESS(ES) N/A	10. SPONSORING/MONITORING AGENCY REPORT NUMBER

11. SUPPLEMENTARY NOTES The views expressed in this thesis are those of the author and do not reflect the official policy or position of the Department of Defense or the U.S. Government.

12a. DISTRIBUTION / AVAILABILITY STATEMENT Approved for public release; distribution is unlimited	12b. DISTRIBUTION CODE A

13. ABSTRACT (maximum 200 words)

The free electron laser (FEL) is among the latest technologies of interest to the U.S. military, in particular, the Navy. In naval applications, FEL laser would serve as a self-defense weapon system, protecting the ship from an array of threats including anti-surface cruise missiles and small boats. This system's potential range and deep magazine makes it ideal as point defense against incoming missiles. Its inexpensive cost of only a few dollars per engagement and multi-mission capability makes this future weapon system superior to the short-range missile-defense systems employed today. The most powerful FEL is currently located in Jefferson Lab, operating at 10 kW, two orders of magnitude short of the 1 MW power level required for weapons application. This thesis will describe the components and theory of operation of the FEL, as well as analyze two competing designs for the next step in the evolution of the future weapon system, the 100 kW FEL, proposed by Brookhaven and Los Alamos National Labs. Due to advances in NPS simulation techniques for the amplifier configuration, a more in depth analysis including the effects of electron beam tilt and shift is performed for the first time on these proposed designs.

14. SUBJECT TERMS Free Electron Laser, High Energy Lasers, FEL, Amplifier, High Power Lasers	15. NUMBER OF PAGES 76
	16. PRICE CODE

17. SECURITY CLASSIFICATION OF REPORT	18. SECURITY CLASSIFICATION OF THIS PAGE	19. SECURITY CLASSIFICATION OF ABSTRACT	20. LIMITATION OF ABSTRACT
Unclassified	Unclassified	Unclassified	UL

NSN 7540-01-280-5500 Standard Form 298 (Rev. 2-89)
Prescribed by ANSI Std. 239-18

THIS PAGE INTENTIONALLY LEFT BLANK

Approved for public release; distribution is unlimited

High-Power Amplifier Free Electron Lasers

Tyrone Y. Voughs
Lieutenant, United States Navy
B.S.E Computer Engineering, University of Michigan, 1999

Submitted in partial fulfillment of the
requirements for the degree of

MASTER OF SCIENCE IN APPLIED PHYSICS

from the

NAVAL POSTGRADUATE SCHOOL
June 2006

Author: Tyrone Y. Voughs

Approved by: William B. Colson
Thesis Advisor

Robert L. Armstead
Co-Advisor

James Luscombe
Chairman, Department of Physics

THIS PAGE INTENTIONALLY LEFT BLANK

ABSTRACT

The free electron laser (FEL) is among the latest technologies of interest to the U.S. military, in particular, the Navy. In naval applications, FEL laser would serve as a self-defense weapon system, protecting the ship from an array of threats including anti-surface cruise missiles and small boats. This system's potential range and deep magazine makes it ideal as point defense against incoming missiles. Its inexpensive cost of only a few dollars per engagement and multi-mission capability makes this future weapon system superior to the short-range missile-defense systems employed today. The most powerful FEL is currently located in Jefferson Lab, operating at 10 kW, two orders of magnitude short of the 1 MW power level required for weapons application. This thesis will describe the components and theory of operation of the FEL, as well as analyze two competing designs for the next step in the evolution of the future weapon system, the 100 kW FEL, proposed by Brookhaven and Los Alamos National Labs. Due to advances in NPS simulation techniques for the amplifier configuration, a more in depth analysis including the effects of electron beam tilt and shift is performed for the first time on these proposed designs.

THIS PAGE INTENTIONALLY LEFT BLANK

TABLE OF CONTENTS

LIST OF FIGURES

LIST OF TABLES

THIS PAGE INTENTIONALLY LEFT BLANK

ACKNOWLEDGMENTS

I'd like to thank the following people for their aid in my preparing this work, without them I would be lost. First, is Professor Colson; whose words of encouragement provided the motivation I needed to complete this thesis. Next, are Professors Armstead, Blau, and Crooker, who all reviewed portions of my writing and provided much needed input to improve its scientific clarity. I would also like to thank both Dinh Ngyuen and Ilan Ben-Zvi from Los Alamos and Brookhaven National Labs respectively for providing the parameters for the FEL simulations and tours of your facilities. But last, and certainly not least, is my wife, who was my rock through the whole process, giving me constant encouragement and hope, comfort when needed. She handled the day to day operations of the household, freeing me to focus more on the task at hand.

THIS PAGE INTENTIONALLY LEFT BLANK

I. INTRODUCTION

A. HISTORY OF THE FREE ELECTRON LASER

The free electron laser (FEL) is among the latest technologies of interest to the U.S. military, in particular, the Navy. In naval applications, FEL laser would serve as a self-defense weapon system, protecting the ship from an array of threats including anti-surface cruise missiles and small boats. This system's potential range of six to ten kilometers and deep magazine makes it ideal as point defense against incoming missiles. Its inexpensive cost of only a few dollars per engagement along with a multi-mission capability versus using a multi-million dollar missile per engagement makes this future weapon system superior to the short-range missile-defense systems employed today.

The FEL is another product in a long line of methods of generating coherent electromagnetic energy, all of which prove quite useful today. The first of these techniques, developed in the 1880's, was the antenna. The antenna emits energy in the form of radio waves directionally and coherently, generated by oscillating currents in metal and wire. The primary purpose of the antenna was the transmission and receipt of radio signals. Through the years, antennae have retained this function in communications and have been utilized in the entertainment industry in the service of radio and television. They now serve as the backbone of all wireless telephone and broadcast television networks worldwide.

The concept of coherent emission was later applied to the microwave region of the electromagnetic spectrum in the creation and development of microwave tubes. The microwave tube was first used in the 1930's, primarily for communication and radar systems. The microwave tube marked the beginning of coherent energy generation in a closed container. The radiation in the closed cavity interacted with the relatively slow moving, non-relativistic electrons. The resulting radiation had long wavelengths on the order of millimeters. The tubes were very efficient, utilizing better than half of the energy supplied as input. The most common use for these tubes now is in an appliance found in the kitchens of almost every home nationwide, the microwave oven. Building and improving upon the concept of microwave tubes, the Microwave Amplification of

Stimulated Emission of Radiation, or MASER was built and developed by Charles H. Townes in 1954 [1].

The stimulated amplification of radiation was later used to produce shorter wavelength radiation in the visible region of the spectrum. This gave rise to the Light Amplification of Stimulated Emission of Radiation or what we commonly call the laser. Theodore H. Maiman built the first working laser in 1960 [1]. Throughout the 1960's, several types of lasers were produced using electrons bound in various atoms and molecules such as ruby, uranium, helium-neon, semiconductor materials, and carbon dioxide. The conventional laser now comes in all shapes and sizes and is commonplace in society, including laser pointers, printers, compact-disc players, DVD players, product scanners and even as instruments in medical procedures.

With all the promise of the conventional laser, it also had shortcomings. These lasers had short wavelengths, but they were not tunable. Bound electrons transitioning from excited to lower energy states determined the wavelengths of these lasers. They were restricted by the energy levels of the atom or molecule that the laser is based upon. Adjustment of wavelength was not possible. Furthermore, these lasers were not as efficient as their predecessors in the microwave regime.

The issue of tunability and efficiency of lasers was addressed in 1971 by John Madey [2]. His invention, the FEL, combined the benefits of both the earlier lasers and the MASER, providing short wavelengths and relatively high efficiency. With the evolution of technology through the years, the free electron laser has been improved upon throughout the world and has most recently achieved a power level as high as ten kilowatts. This laser is currently in operation at Jefferson Lab in Newport News, Virginia.

B. ADVANTAGES OF THE FREE ELECTRON LASER

One of the major advantages of the FEL over other lasers is its flexibility of design. In conventional lasers, the operating wavelength is predetermined by the chemical composition of the lasing medium. In contrast, the basic components of the FEL can be used in the microwave, infrared, visible, ultraviolet, and X-ray regions of the electromagnetic spectrum. Furthermore, with a given configuration, the free electron

laser has an ability to be finely tuned in operating wavelength. To accomplish this, one would only have to change the electron beam energy through adjustment of the intensity of the electric fields in the radio frequency (RF) accelerator or injector. Free electron lasers are capable of running twenty-four hours a day for weeks at a time. Another advantage of the free electron laser over conventional lasers is cost of operation. For example, in high-power conventional chemical lasers, the chemical being used as the lasing medium is spent and exhausted during operation. Since the chemical, usually toxic, is being expelled, it must be replenished after repeated use for the laser to operate. The FEL does not suffer from this shortcoming. As long as sufficient power is supplied to the system, and none of the components are damaged, the free electron laser will operate. There is no exhaust gas involved in the process of lasing, thus no need for replenishment and no danger to people or the environment.

The one drawback of the FEL is the fact that the system tends to be quite large and expensive, but only compared to the conventional laser at low power. Any MW-level conventional laser will have a comparable large cost. The size of the FEL does not scale linearly with output power (i.e. a 10kW FEL is not one-tenth the size of a 100kW FEL). Furthermore, advances in FEL designs incorporating technologies such as superconducting RF accelerators and application of concepts including short Rayleigh lengths, will reduce the size of the system.

THIS PAGE INTENTIONALLY LEFT BLANK

II. FREE ELECTRON LASER SYSTEM COMPONENTS

A. INTRODUCTION

There are several components that make up the total free electron laser system. Many supporting elements are used for cooling, input power, and other functions, but for brevity the focus will be limited to the major components of the system. The basic system is comprised of an injector to provide the electron beam, an accelerator to raise the electron beam to a useful energy level, an undulator to extract light energy from the electron beam, a resonator to store light created, a beam dump to dispose of the used electrons, and bending magnets to route the electron beam through the system to each of components. A schematic of the free electron laser system at Jefferson Laboratory is shown in Figure 1 below.

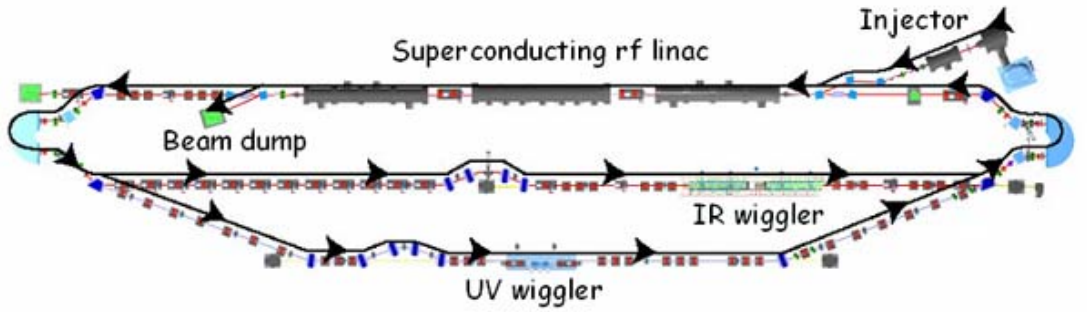

Figure 1. Diagram of Jefferson Lab free electron laser system ([From Ref [3].)

B. INJECTOR

The electron beam formation begins at the injector where free electrons are emitted from a cathode. Four types of injectors are: thermionic, direct current (DC), radio frequency (RF) and superconducting RF. The thermionic gun utilizes heat energy to excite electrons in a cathode (a metal plate), providing the source of electrons used in the system. This cathode, when heated, releases electrons. The RF and DC injectors accomplish the same using the photoelectric effect; a laser illuminates the cathode, and the cathode absorbs the light. This absorbed energy excites electrons in the cathode, causing it to release the electrons. The newly-freed low energy electrons are given additional energy and accelerated to relativistic velocities by the injector. The beam is

typically accelerated to only modest energy levels (2-10 MeV) in the injector. A schematic of the injector is shown below in Figure 2.

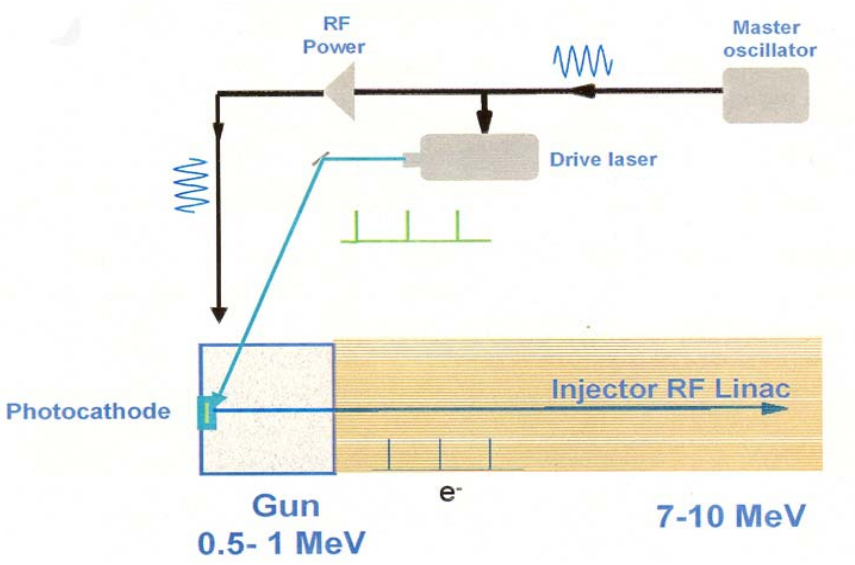

Figure 2. Schematic for an RF injector gun ([From Ref. [4].)

C. ACCELERATOR

After leaving the injector, the free electrons are relativistic but still remain at too low an energy to be useful for weapons application. The accelerator (shown in Figure 3 below) gives the electron pulses the additional energy needed for the desired power output of the laser. The accelerator is a series of cavities into which RF energy is fed and alternating electric fields are set up. The size of cavities roughly determines the frequency of operation of the system. The number of cavities in the accelerator roughly determines the amount of RF energy in the accelerator. During operation, electrons go through each cavity in the accelerator and are exposed to the alternating electric fields that are present. When the electrons are coming from the injector in phase with the electric field, they absorb energy from it. This energy absorption accelerates and bunches the electrons, and slightly reduces the electric field present in the cavity, so the RF energy must be replenished to continue operation. The power requirement to replenish the electric fields is reduced by the recirculation of electrons through the system. Electrons that have gone through the undulator can be sent through the accelerator for a second

time, now out of phase with the electric field in each cavity. The electrons then lose energy and replenish the RF electric fields.

Figure 3. An example of a RF accelerator ([From Ref. [5].)

D. UNDULATOR

Once emerging from the accelerator, the electron beam is at a high energy (approximately 100 MeV). The electron beam energy is the source of energy for the laser light. Extraction of energy from the electron beam and amplification of light are accomplished in the undulator. The undulator (shown in Figure 4) is constructed from two rows of adjacent permanent magnets with alternating poles. The magnets are oriented so that there is an alternating static magnetic field along the undulator axis. Upon entry into the undulator, the electrons experience Lorentz forces due to the magnetic fields. The Lorentz forces cause the electrons to oscillate with small amplitude. These small oscillations cause the electrons to emit radiation in the form of light. The light emitted by the electrons interacts with the light stored in the undulator through stimulated emission, which amplifies the light already present in the undulator. The undulator typically extracts only a few percent of the energy from the electron beam for output laser light. The rest of the electron beam's energy is recirculated and routed back to the accelerator for increased system efficiency.

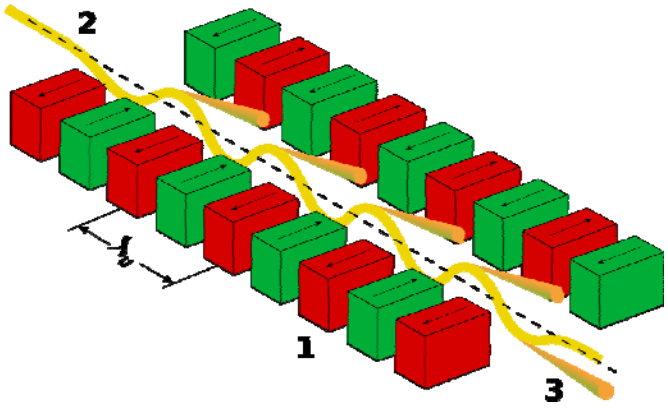

Figure 4. A schematic of an undulator ([From Ref. [6].)

E. OSCILLATOR RESONATOR

The oscillator configuration is equipped with a resonator to store and amplify light through many passes. The resonator consists of an evacuated cavity terminated by two specially constructed mirrors. One mirror is almost perfectly reflective, while the second, the out-coupling mirror, is partially transmissive, allowing a fraction of the light to pass through it and escape the resonator as a usable laser light source. The undulator is typically placed halfway between the mirrors. Light bounces between the two mirrors at the operating wavelength and is amplified between each bounce by the undulator through stimulated emission due to its interaction with the electron beam.

F. AMPLIFIER SEED LASER

The amplifier configuration of the FEL uses a long undulator to amplify a coherent light source in a single pass. Therefore, the amplifier design has no resonator mirrors and no ability to store light. The amplifier employs a seed laser as a source of light to be amplified by the undulator. A low-power, solid-state laser usually serves as the seed laser for an amplifier FEL system.

G. BENDING MAGNETS

In the recirculating electron beam design of the FEL system, there are bends in the system where the electron beam must be routed around components. A high power electron beam incident on either of the resonator mirrors, the injector, or the system piping itself would prove disastrous to the operation of the system. Bending magnets provide the means of routing the electron beam through the system piping around these components. The powerful bending magnets are configured so that the electron beam,

when passing through them, is deflected by the Lorentz forces resulting from the magnetic fields. Bending magnets provide an extremely tight control of the electron beam direction. However, the full recirculation through the bending magnets requires that the electron beam has a small energy spread to ensure efficient operation.

E. BEAM DUMP

Once the electron beam has passed through the undulator and has lost energy, it is routed through bending magnets back to the accelerator. Even though the electrons have lost a few percent of their energy in the undulator, they still have much more energy than those emerging from the injector. The higher energy electrons by design arrive at the accelerator out of phase with the electric fields. Going through the accelerator out of phase has the opposite effect on the electrons causing them to lose energy to the accelerator. The accelerator decelerates the spent electrons in preparation for disposal bringing them to a level roughly that of electrons exiting the injector. Though at a much lower energy, the electrons still have energy that must be absorbed, which is the purpose of the beam dump. It is basically a block of metal, which just absorbs electrons incident on it. Along with absorbing energy, it absorbs heat and potentially harmful radiation. A beam dump used by the FEL system at Jefferson Lab is shown below in Figure 5. Care must be taken to cool and shield this component in the system.

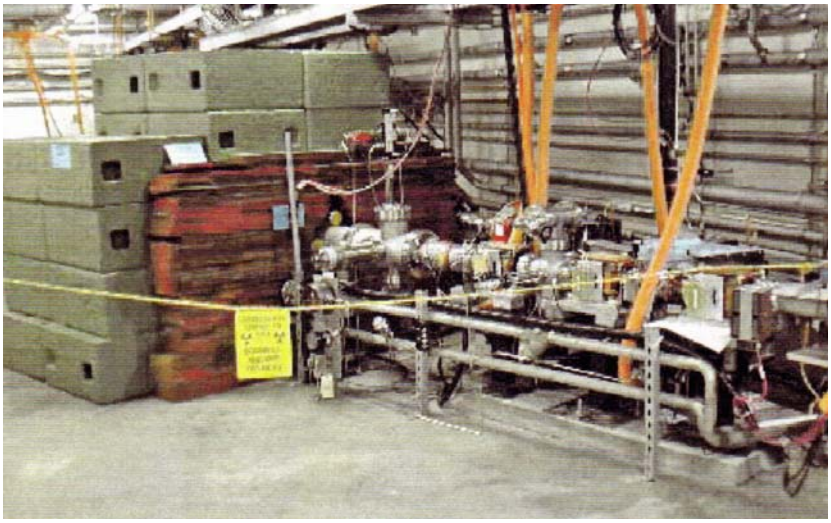

Figure 5. Jefferson Lab Beam Dump ([From Ref. [4].)

THIS PAGE INTENTIONALLY LEFT BLANK

III. FREE ELECTRON LASER BASIC THEORY

A. INTRODUCTION

Of all components in the free electron laser, the most physics concepts emerge from the study of electrons and light propagating together through the undulator. The interaction of the laser light and electron beam present in the undulator is crucial to the proper operation of an FEL. This section mathematically describes the process of laser light amplification and propagation along the undulator.

B. LORENTZ FORCE EQUATIONS

When the electrons enter the undulator, they are exposed to a transverse, periodic magnetic field. For a helical undulator, this magnetic field is,

$$\vec{B} = B(\cos(k_0 z), \sin(k_0 z), 0). \tag{III.1}$$

In this equation, B represents the magnetic field strength and k_0 is the wavenumber corresponding to the undulator period ($k_0 = 2\pi / \lambda_0$). The undulator period λ_0 is the distance between two successive, identically oriented magnets in the undulator.

Along with the magnetic field due to the undulator magnets, electrons are influenced by the magnetic and electric fields of the laser light, which (in cgs units) are represented by

$$\vec{E} = E(\cos\psi, -\sin\psi, 0), \tag{III.2}$$

$$\vec{B} = E(\sin\psi, \cos\psi, 0), \tag{III.3}$$

$$\psi = kz - \omega t + \phi. \tag{III.4}$$

In these equations, E represents the optical electric field amplitude, k is the wavenumber related to the optical wavelength λ ($k = 2\pi / \lambda$), $\omega = kc = 2\pi c / \lambda$ is the optical frequency, and ϕ is the optical phase.

A charged particle going through electric and magnetic fields encounters a force that acts upon it given by the Lorentz force equation. For relativistic particles, the complete Lorentz FEL force equations for electrons in the undulator are given by

$$\frac{d(\gamma\vec{\beta})}{dt} = -\frac{e}{mc}(\vec{E} + \vec{\beta} \times \vec{B}), \tag{III.5}$$

$$\frac{d\gamma}{dt} = -\frac{e}{mc}\vec{\beta} \cdot \vec{E}, \tag{III.6}$$

$$\gamma^{-2} = 1 - \vec{\beta}^2. \tag{III.7}$$

In these equations, -*e* represents the electron charge, *m* the electron mass, $\vec{E}$ is the electric field, $\vec{B}$ is the magnetic field, $\vec{\beta}$ is dimensionless and proportional to the electron velocity ($\vec{\beta} = \vec{v}/c$), where c is the speed of light, and γ is the relativistic Lorentz factor appearing in the total electron energy γmc^2.

C. ELECTRON MOTION IN THE ABSENCE OF LIGHT IN UNDULATOR

Electron motion in the undulator is first studied without the presence of light. Since there is no light in the undulator, there is no electric field ($\vec{E} = 0$), and the force equations revert to the simplest form. With no light in the undulator, equations III.5 and III.6 become

$$\frac{d(\gamma\vec{\beta})}{dt} = -\frac{e}{mc}(\vec{\beta} \times \vec{B}), \tag{III.8}$$

$$\frac{d\gamma}{dt} = 0. \tag{III.9}$$

Equation III.9 shows that the magnetic field does no work on the electrons and the electron energy (γmc^2) remains constant. Substituting the helical undulator magnetic field (equation III.1) into equation III.8 results in

$$\frac{d(\gamma\vec{\beta})}{dt} = -\frac{eB}{mc}(-\beta_z \sin(k_0 z), \beta_z \cos(k_0 z), \beta_x \sin(k_0 z) - \beta_y \cos(k_0 z)). \tag{III.10}$$

Equation III.10 shows that the motion of the electrons in both the x and y directions is sinusoidal in nature with only a phase difference between them. Integrating the transverse components of equation III.11 gives the transverse velocity ($\vec{\beta}_\perp = (\beta_x, \beta_y, 0)$) of the electrons,

$$\vec{\beta}_{\perp} = -\frac{eB\lambda_0}{2\pi\gamma mc^2}(\cos(k_0 z), \sin(k_0 z), 0). \quad \text{(III.11)}$$

In equation III.11, all integration constants are zero, indicating perfect injection into the undulator. A more compact form of this equation is given by equation III.12, where $K = eB\lambda_0 / 2\pi mc^2$ is the dimensionless undulator parameter. The value of the undulator parameter is typically on the order of unity ($K \approx 1$), so that

$$\vec{\beta}_{\perp} = -\frac{K}{\gamma}(\cos(k_0 z), \sin(k_0 z), 0). \quad \text{(III.12)}$$

Since the electrons in the undulator are highly relativistic, the velocity of the electrons can be approximated as the speed of light. Therefore, the approximation ($z(t) \approx \beta_z ct \approx ct$) is reasonable. Substitution of this approximation yields

$$\vec{\beta}_{\perp} = -\frac{K}{\gamma}(\cos(\omega_0 t), \sin(\omega_0 t), 0). \quad \text{(III.13)}$$

In this equation, $\omega_0 = k_0 c$ represents the electron oscillation frequency. Integration of equation III.13 describes the transverse motion of the electrons in the undulator,

$$\vec{x}_{\perp} = \frac{K\lambda_0}{2\pi\gamma}(-\sin(\omega_0 t), \cos(\omega_0 t), 0). \quad \text{(III.14)}$$

D. ELECTRON MOTION IN THE UNDULATOR WITH LASER LIGHT INTERACTION

Both motion and energy exchange of the electrons in the undulator with laser light can be described by using the aforementioned complete relativistic Lorentz FEL force equations with the magnetic and electric fields due to the light in the undulator. Substitution of the magnetic and electric fields into equation III.5 yields

$$\frac{d(\gamma\vec{\beta}_{\perp})}{dt} = -\frac{e}{mc}[E(1-\beta_z)(\cos\psi, -\sin\psi, 0) + \beta_z B(-\sin(k_0 z), \cos(k_0 z), 0)], \quad \text{(III.15)}$$

$$\frac{d(\gamma\beta_z)}{dt} = -\frac{e}{mc}[E(\beta_x \cos\psi - \beta_y \sin\psi) + B(\beta_x \sin(k_0 z) - \beta_y \cos(k_0 z))]. \quad \text{(III.16)}$$

In these equations, β_z represents the magnitude of the longitudinal z component of the electron velocity, $\beta_\perp$ represents the transverse x and y components, and β_x and β_y are the x and y components of the velocity, respectively.

The electrons going through the undulator are highly relativistic, so their velocities along the axis of the undulator z-axis are very close to the speed of light. This causes β_z to be very close to but less than one. Applying this condition to equation III.15 makes the electric field term negligible compared to the magnetic field term. Integration of equation III.15 approximately results in equation III.11 and one can proceed as in the case of electron motion in the absence of light to describe the transverse motion of electrons in the undulator.

In studying the microscopic variation of motion of the electron along the undulator axis, equation III.6 is utilized, substituting the transverse velocity (equation III.12) for β_x and β_y. The result is

$$\frac{d\gamma}{dt} = \dot{\gamma} = -\frac{e}{mc}\vec{\beta}\cdot\vec{E} = \frac{eKE}{\gamma mc}(\cos k_0 z\cos\psi - \sin k_0 z\sin\psi) = \frac{eKE}{\gamma mc}\cos(\zeta+\phi), \qquad \text{(III.17)}$$

where $\zeta = (k+k_0)z - \omega t$ represents the electron phase. The electron phase follows the microscopic position with respect to the undulator field and the co-propagating optical field and is proportional to $z(t)$. The electron phase closely corresponds to the electron's position within an optical wavelength. The first and second derivatives of the electron phase are taken with respect to the dimensionless time $\tau = ct/L$,

$$\overset{\circ}{\zeta} = \frac{d\zeta}{d\tau} = \frac{d\zeta}{dt}\frac{L}{c},$$

$$\overset{\circ\circ}{\zeta} = \frac{d^2\zeta}{d\tau^2} = \frac{d^2\zeta}{dt^2}\frac{L^2}{c^2},$$

where L is the length of the undulator. The time derivative of the electron phase gives the electron phase velocity

$$\nu = \overset{\circ}{\zeta} = L[(k+k_0)\beta_z - k].$$

An expression for β_z is found by squaring the expression for the transverse velocity (equation III.13), combining that result with the square of the z component of the velocity ($\vec{\beta}^2 = \beta_\perp^2 + \beta_z^2$) and substituting into equation III.7. The result is the following equation, relating the electron energy to its z-component of velocity,

$$\beta_z = \sqrt{1 - \frac{(1+K^2)}{\gamma^2}}\,.$$

For highly relativistic electrons ($\gamma \gg 1$), the above equation can be approximated as

$$\beta_z \approx 1 - \frac{1+K^2}{2\gamma^2}\,. \tag{III.18}$$

For relativistic electrons near resonance $k \gg k_0$, the first derivative of the electron phase then becomes

$$\overset{\circ}{\zeta} \approx L\left[(k+k_0)\left(1-\frac{1+K^2}{2\gamma^2}\right)-k\right] \approx -Lk\left(\frac{1+K^2}{2\gamma^2}\right).$$

Taking the second derivative yields

$$\overset{\circ\circ}{\zeta} = \frac{\dot{\gamma} k L^2}{c}\left(\frac{1+K^2}{\gamma^3}\right). \tag{III.19}$$

Substitution of equation III.17 for $\dot{\gamma}$ in the above equation gives the dimensionless pendulum equation,

$$\overset{\circ\circ}{\zeta} = \overset{\circ}{\nu} = |a|\cos(\zeta + \phi)\,, \tag{III.20}$$

where $|a|$ represents the dimensionless optical field amplitude $|a| = 4\pi NeKL|E|/\gamma^2 mc^2$. Values for $|a|$ that are less than π are considered weak fields and those that are greater than or equal to π are strong fields. This dimensionless pendulum equation describes the microscopic motion of electrons within the undulator.

E. FEL RESONANCE CONDITION

Equation III.17 describes not only the longitudinal motion; it also describes the energy exchange between the electrons and the laser light in the undulator. If the factor $\cos(\zeta + \phi)$ is positive, then the electron energy increases; if it is negative, the energy decreases. For effective energy exchange, the factor must not oscillate rapidly in the time that the electron takes to go through the undulator, $L/\beta_z c \approx L/c$. Electron phase velocity ($\nu = \dot{\zeta} L / c = L[(k + k_0\beta_z - k)] = \overset{\circ}{\zeta}$) is the rate of change of the electron phase with respect to the dimensionless time.

When the phase velocity is equal to zero, the free electron laser is at resonance and there is an optimal energy exchange between the electrons and laser optical field. It occurs when the electron velocity along the axis of the undulator, $\beta_z c$, is equal to $kc/(k + k_0)$. For high-energy electrons, $\beta_z \approx 1$ and $k \gg k_0$, so the corresponding wavelength of the laser light, $\lambda = 2\pi/k$, is much smaller than the period of the undulator, $\lambda_0 = 2\pi/k_0$. In addition, the oscillation frequency of the laser light, $\omega = 2\pi c/\lambda$, is much greater than the electron oscillation frequency, $\omega_0 = 2\pi c/\lambda_0$, in the undulator. Solving the resonance condition for laser wavelength gives

$$\lambda = \lambda_0(1 - \beta_z)/\beta_z . \tag{III.21}$$

A more useful form of the resonance equation is obtained by substitution of equation III.18 into equation III.21. The result is

$$\lambda \approx \frac{\lambda_0(1 + K^2)}{2\gamma^2} . \tag{III.22}$$

F. FEL PHASE SPACE

In a typical free electron laser, there are approximately a million electrons randomly spread over each wavelength of light in the electron beam. Each electron in the electron beam has its own initial phase and phase velocity (ζ_0, ν_0) when entering the undulator. The electron phase ζ_0 measures the position of the electron in the beam on the scale of the length of the laser wavelength, while the phase velocity ν_0 is proportional to the energy of the electron. By examining the FEL pendulum equation (equation

III.20), one sees that the electron will either gain or lose energy depending on its particular initial phase and phase velocity. To graphically aid in the study of the electron evolution within the undulator, the electrons are plotted using a phase space consisting of the electron phase and phase velocity (ζ, ν). This method graphically identifies the electrons losing energy (decreasing ν) or gaining energy (increasing ν), and simultaneously shows how the electrons evolve in phase ζ. Given initial conditions, the electron path is predetermined in phase space in accordance with the pendulum equation. Substitution of the initial conditions and application of the pendulum equation gives the phase space path of an electron

$$\nu^2 = \nu_0^2 + 2|a|\left[\sin(\zeta + \phi) - \sin(\zeta_0 + \phi)\right]. \tag{III.23}$$

Since some of the electrons are gaining energy while some are losing energy, electron bunching in each wavelength may and often does occur. This phenomenon is easily seen with the use of phase space. Figure 6 is an example of a phase space plot of an idealized FEL with 20 sample electrons exactly at resonance ($\nu_0 = 0$) with zero optical phase ($\phi = 0$) and weak field amplitude $|a| = a_0 = 2$. The separatrix is plotted in red and the paths of the electron are plotted with a yellow to red gradient. The separatrix is the path that separates closed orbits (analogous to a pendulum swinging back and forth) from open orbits (analogous to the pendulum going over the top and swinging in a full circle) and is given by

$$\nu^2 = 2|a|\left[1 + \sin(\zeta + \phi)\right]. \tag{III.24}$$

The height of the separatrix is determined by the strength of the optical field $2\sqrt{|a|} = 2\sqrt{2}$. The final electron positions are represented in blue. This plot illustrates there is an optimal energy exchange at resonance, with some electrons gaining and some losing energy. The higher energy electrons catch up to those with lower energy, and bunching occurs as shown by the decrease of spacing between the electrons toward the center in the figure below. However, in this case, an equal number of electrons gain and lose energy, resulting in a net energy change in the electron beam of nearly zero. There is then negligible gain G in the intensity of the laser light.

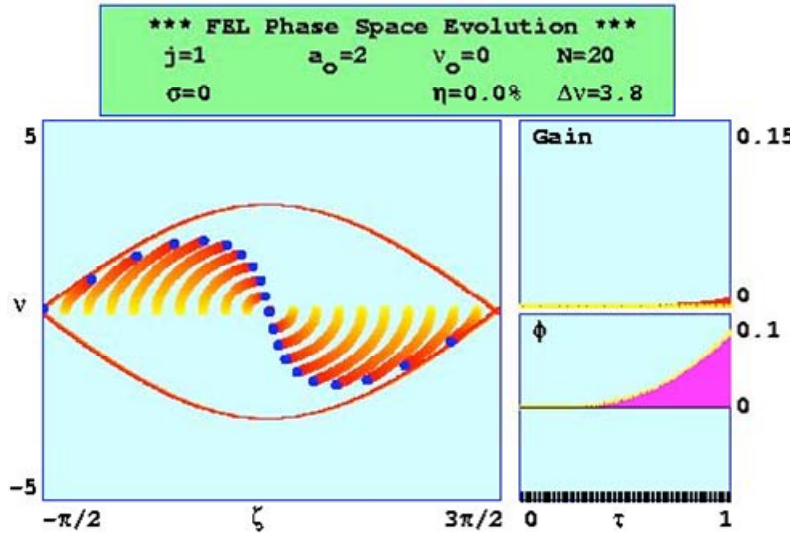

Figure 6. FEL Phase Space Plot at Resonance ($\nu_0 = 0$) ([From Ref. [4].)

A more desirable phase space plot of an operating FEL is shown in Figure 7. In this simulation, 1000 sample electrons start out at energies slightly above resonance ($\nu_0 = 3$). There is energy exchange between the electrons and the light, but more electrons lose energy than gain energy, which is desirable since the energy lost by the electrons is gained by the light. There is also a bunching of electrons that are losing energy, leading to coherent radiation, another desired characteristic of a free electron laser.

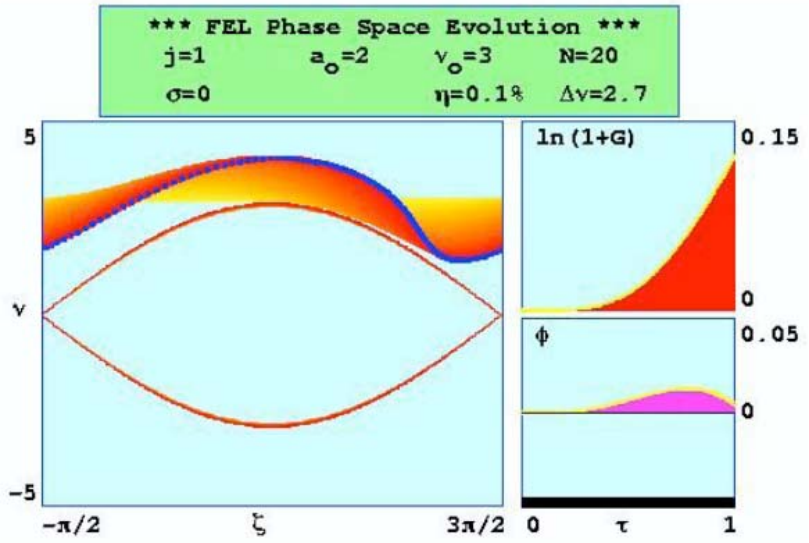

Figure 7. Phase Space Above Resonance ($\nu_0 = 3$) ([From Ref. [4].)

G. DIFFRACTION OF THE LASER BEAM

Propagation of a light wave can be mathematically described using the wave equation given by

$$\left(\vec{\nabla}^2 - \frac{1}{c^2}\frac{\partial^2}{\partial t^2}\right)E(\vec{x},t) = 0\,. \tag{III.25}$$

This equation involves four second order derivatives in $(\vec{x},t)$ for the propagation of the light, with $E(\vec{x},t)$ representing the electric field of the light. In a typical operating FEL, the light is highly coherent and the electric field due to the light is slowly varying in the direction of travel (z axis) over an optical wavelength and slowly varying in time over the optical frequency. The complex electric field is then represented by

$$E(\vec{x},t) = a(x,t)e^{i\alpha} = \left|a(\vec{x},t)\right|e^{i\phi(\vec{x},t)}e^{i\alpha} \text{ [7].} \tag{III.26}$$

In this equation, $\alpha = kz - \omega t$ represents the carrier wave and the optical field is represented by $a = \left|a\right|e^{i\phi}$. If the optical field is constant in magnitude, then the electric field E describes a simple plane wave traveling in the z direction containing a single frequency ω. Because the laser amplitude and phase are slowly varying, we can make the following assumptions describing the two

$$\frac{\partial|a|}{\partial t} \ll \omega|a|,\ \frac{\partial|a|}{\partial z} \ll k|a|,\ \frac{\partial\phi}{\partial t} \ll \omega\phi,\ \frac{\partial\phi}{\partial z} \ll k\phi\,.$$

Substituting the expression for $E(\vec{x},t)$ into the wave equation, gives

$$\left[\nabla_\perp^2 a + \left(\frac{\partial^2 a}{\partial z^2} + 2ik\frac{\partial a}{\partial z} - k^2 a\right) - \frac{1}{c^2}\left(\frac{\partial^2 a}{\partial t^2} - 2i\omega\frac{\partial a}{\partial t} - \omega^2 a\right)\right]e^{i\alpha} = 0\,, \tag{III.27}$$

where $\nabla_\perp^2 = \frac{\partial^2}{\partial x^2} + \frac{\partial^2}{\partial y^2}$ is the transverse Laplacian. Because of the slowly varying amplitude and phase assumptions, we may simplify the equation by neglecting the second derivative terms. Multiplying the simplified equation by the factor $e^{-i\alpha}$ results in

$$\left[\nabla_{\perp}^{2} + 2ik\left(\frac{\partial}{\partial z} + \frac{1}{c}\frac{\partial}{\partial t}\right)\right] a(\vec{x},t) = 0\,. \qquad \text{(III.28)}$$

This equation is simplified further by introducing another coordinate $u = z - ct$ that follows the wavefront. The partial derivatives are now

$$\frac{\partial}{\partial z} = \frac{\partial u}{\partial z}\frac{\partial}{\partial u} + \frac{\partial t}{\partial z}\frac{\partial}{\partial t} = \frac{\partial}{\partial u},$$
$$\frac{1}{c}\frac{\partial}{\partial t} = \frac{1}{c}\left(\frac{\partial u}{\partial t}\frac{\partial}{\partial u} + \frac{\partial t}{\partial t}\frac{\partial}{\partial t}\right) = -\frac{\partial}{\partial u} + \frac{1}{c}\frac{\partial}{\partial t}.$$

Substitution of the derivative forms using the new coordinate now gives the wave equation a new form

$$\left[\nabla_{\perp}^{2} + \frac{2ik}{c}\frac{\partial}{\partial t}\right] a(\vec{x},t) = 0\,. \qquad \text{(III.29)}$$

A dimensionless time variable is then defined relating to the travel time of the laser light along the undulator $\tau = ct/L$, where L is the undulator length. This time variable ranges from $\tau = 0$ at the beginning of the undulator to $\tau = 1$ at the end of the undulator. Introduction of this variable results in

$$\left[\left(\frac{-iR}{2k}\right)\nabla_{\perp}^{2} + \frac{\partial}{\partial \tau}\right] a(\vec{x},t) = 0\,. \qquad \text{(III.30)}$$

The first term in equation III.30 is the diffraction term, and its magnitude depends on the transverse area of the laser beam, its wavelength, $\lambda = 2\pi / k$ and the range to the target. The Rayleigh length Z_0 is defined as the distance from the mode waist to where the area of the optical mode doubles due to diffraction. This length relates the optical mode waist radius W_0 to the wavelength of the light by the following: $Z_0 = \pi W_0^2 / \lambda$. In defining dimensionless variables for transverse coordinates, Z_0 is taken to be equal to the length of the undulator L. The characteristic mode waist radius is $\sqrt{L\lambda/\pi} = \sqrt{2L/k}$. When the optical mode radius is much larger than $\sqrt{L\lambda/\pi}$, then diffraction has a small effect over the range of propagation, if it is smaller than $\sqrt{L\lambda/\pi}$, diffraction has a big effect in propagation to the target. Dimensionless coordinates based on the characteristic

mode waist radius are $\tilde{x} = x\sqrt{k/2L}$ and $\tilde{y} = y\sqrt{k/2L}$. Substitution of these dimensionless variables yields a totally dimensionless form of the wave equation

$$\frac{\partial a}{\partial \tau} = \frac{i}{4}\tilde{\nabla}_{\perp}^{2} a\,, \tag{III.31}$$

where $\tilde{\nabla}_{\perp}^{2} = \frac{\partial^2}{\partial \tilde{x}^2} + \frac{\partial^2}{\partial \tilde{y}^2}$. When the transverse components $(\tilde{x}, \tilde{y})$ of the laser beam are on the order of unity or smaller, diffraction has a significant effect over the propagation range ($\tau = 0 \rightarrow 1$); if they are much greater than unity, diffraction has little effect and can be neglected. Diffraction causes both the amplitude and phase of the optical field to evolve.

H. FEL WAVE EQUATION

The FEL wave equation describes the evolution of the optical field interacting with the electron beam within the undulator. The wave equation with a current source $\vec{J}_{\perp}$ is

$$\left(\nabla_{\perp}^{2} - \frac{1}{c^2}\frac{\partial^2}{\partial t^2}\right)\vec{A}(\vec{x},t) = -\frac{4\pi}{c}\vec{J}_{\perp}(\vec{x},t)\,. \tag{III.32}$$

In this equation, $\vec{A}(\vec{x},t)$ represents the optical vector potential. The laser electric field can be obtained from this potential by

$$\vec{E} = -\frac{1}{c}\frac{\partial \vec{A}}{\partial t}\,. \tag{III.33}$$

As before, the optical field is coherent laser light so $E(\vec{x},t)$ is complex and slowly varying in amplitude and phase over a laser wavelength and slowly varying in time compared to the optical frequency. The vector potential is given by

$$\vec{A}(\vec{x},t) = \frac{E(\vec{x},t)}{k}\hat{\varepsilon}e^{i\alpha}\,. \tag{III.34}$$

As before, $\alpha = kz - \omega t$ represents the carrier wave, and $\hat{\varepsilon}$ is the laser polarization vector (circularly polarized due to the helical undulator, $\hat{\varepsilon} = (-i, 1, 0)$). Using the slowly varying amplitude and phase assumptions the complete wave equation becomes

$$\frac{\hat{\varepsilon}e^{i\alpha}}{k}\left[\nabla_{\perp}^{2}+2ik\left(\frac{\partial}{\partial z}+\frac{1}{c}\frac{\partial}{\partial t}\right)\right]\vec{E}=-\frac{4\pi}{c}J_{\perp}(\vec{x},t)\,. \tag{III.35}$$

Multiplication of the equation by $ke^{-i\alpha}\hat{\varepsilon}^{*}$, and introduction of the coordinate $u=z-ct$ yields the parabolic wave equation with a current source

$$\left[\nabla_{\perp}^{2}+2ik\left(\frac{1}{c}\frac{\partial}{\partial t}\right)\right]\vec{E}=-\frac{4\pi}{c}\vec{J}_{\perp}(\vec{x},t)\hat{\varepsilon}^{*}e^{i\alpha}\,. \tag{III.36}$$

The current source $\vec{J}_{\perp}=-e\sum_{i}\vec{v}_{\perp}$, where $v_{\perp}=c\beta_{\perp}$ is due to the transverse motion of the electrons in the undulator. Introducing dimensionless variables for time and transverse coordinates ($\tau=ct/L$, $\tilde{x}=x(k/2L)$, and $\tilde{y}=y(k/2L)$) and multiplying by ($-4\pi NeKL^{2}/\gamma_{0}^{2}mc^{2}$) gives the dimensionless wave equation

$$\left[-\frac{i}{4}\tilde{\nabla}_{\perp}^{2}+\frac{\partial}{\partial\tau}\right]a(\vec{x},t)=-<je^{-i\zeta}>_{(\vec{x},t)}\,. \tag{III.37}$$

In this equation, $a=|a|e^{i\phi}$ represents the dimensionless optical field amplitude $|a|=4\pi NeKL|E|/\gamma_{0}^{2}mc^{2}$, j is the dimensionless current $j=8\pi^{2}Ne^{2}K^{2}L^{2}\rho/\gamma_{0}^{3}mc^{2}$, ρ represents the density of electrons in a small volume element, and < > represents the average over all sample electrons in a small volume element. If there is little diffraction in the undulator and the electron and optical beams overlap, the wave equation simplifies to

$$\overset{\circ}{a}=-j<e^{-i\zeta}>\,. \tag{III.38}$$

When $j\gg\pi$, the FEL is operating in the high-gain regime; when $j<\pi$, the FEL is in the low-gain regime. The factor $<e^{-i\zeta}>$ indicates the amount of electron bunching in the undulator.

IV. FREE ELECTRON LASER ADVANCED TOPICS

A. WEAK FIELD GAIN THEORY

Gain in the free electron laser is achieved through the interaction of the bunched electron beam with the optical field in the undulator. This section will derive gain in weak optical fields ($|a| \ll \pi$). The following expressions are valid for weak or strong optical fields

$$\frac{d|a|}{d\tau} = -j < \cos(\zeta + \phi) >, \tag{IV.1}$$

$$\dot{\phi} = \frac{j}{|a|} < \sin(\zeta + \phi) >, \tag{IV.2}$$

where < > represents the average of all the electrons within an optical wavelength of the beam, and describe the change in optical amplitude and phase during FEL operation due to the electron beam interaction. In examining these equations, optimal gain occurs when the factor $< \cos(\zeta + \phi) >$ is approximately negative one. This condition occurs when the electrons are bunched around the phase $\zeta + \phi \approx \pi$.

There are two distinct gain regimes, low and high. These regimes are characterized by the dimensionless current density *j*, describing the coupling between the electron beam and the optical field, as shown in the FEL wave equation (equation III.42) and the above equations. If $j \le \pi$, the system is in the low gain regime; if $j \gg \pi$, it is in the high gain regime.

1. Low Gain Regime

In the low gain regime, *j* is small and there is not an appreciable change in the optical field amplitude or phase as the electrons pass through the undulator. This results in an approximately fixed separatrix when the electron evolution is plotted in phase space. The small change of the optical amplitude and phase as the electron beam goes through the undulator ($\tau = 0 \rightarrow 1$) is given by

$$|a(\tau)| = a_0 \left[1 + j \left(\frac{2 - 2\cos(\nu_0 \tau) - \nu_0 \tau \sin(\nu_0 \tau)}{2\nu_0^3} \right) \right], \tag{IV.3}$$

$$\phi(\tau) = j\left(\frac{2\sin(\nu_0\tau) - \nu_o\tau(1+\cos(\nu_0\tau)}{2\nu_0^3}\right) \text{ [7]}, \qquad \text{(IV.4)}$$

where, a_0 represents the initial optical field amplitude and ν_0 is the initial phase velocity of the electron beam. These equations are obtained by expanding ζ and ν in powers of $|a| = a_0$. Gain in the FEL system is sensitive to initial phase velocity or energy of the electron beam. The electron beam starting at resonance ($\nu_0 = 0$, see Figure 6) yields negligible gain, and initial phase velocities just below resonance ($\nu_0 < 0$) yield negative gain (absorption) in the system. The resulting gain as the electrons go through the undulator is given by

$$G(\tau) = j\left(\frac{2 - 2\cos(\nu_0\tau) - \nu_0\tau\sin(\nu_0\tau)}{\nu_0^3}\right) \text{ [7]}. \qquad \text{(IV.5)}$$

The weak-field, low gain and phase spectra as functions of initial phase velocity are shown below in Figure 8. The gain spectrum is anti-symmetric about the resonance frequency with positive gain for phase velocities just above resonance (see Figure 7). The maximum gain of about 14 percent is achieved with an initial phase velocity of approximately π with $j = 1$. The phase spectrum is symmetric about resonance, where the optical phase shift is at a maximum.

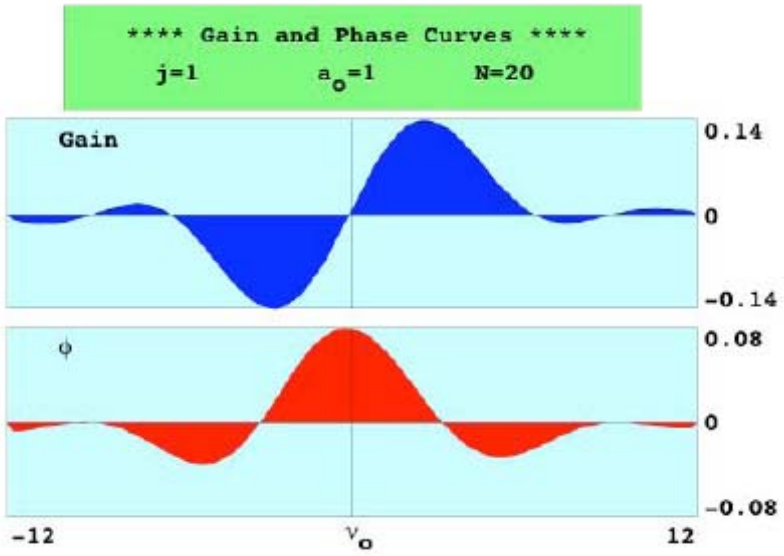

Figure 8. Gain and Phase Spectra for Low-Gain ([From Ref. [4].)

2. High Gain Regime

Unlike the low gain regime, when the dimensionless current density is large ($j \gg \pi$), it strongly affects the optical field amplitude and phase as the electron beam goes through the undulator. The optical field amplitude grows exponentially, and the phase grows linearly. The optical field amplitude and phase during the electron beam interaction with the optical field are given by

$$|a(\tau)| = \frac{a_0}{3} e^{(j/2)^{1/3}\sqrt{3}\tau/2}, \text{ and} \tag{IV.6}$$

$$\phi(\tau) = (j/2)^{1/3}\,\tau/2 \text{ [7].} \tag{IV.7}$$

Because of the large changes in the optical field phase, the separatrix in phase space is shifted and the optimum bunching location changes. The gain spectrum changes as well and the final gain is not as sensitive to initial phase velocity as was the case in the low gain regime. A simulation of an FEL operating in the high gain regime ($j = 200$) with weak fields is shown in Figure 9. In comparison to Figure 7, where the bunching is at a phase of $\zeta \approx \pi$, the separatrix and bunching location has shifted to the left by about π. In this simulation, the electron beam started at resonance ($\nu_0 = 0$), and yet there was considerable gain.

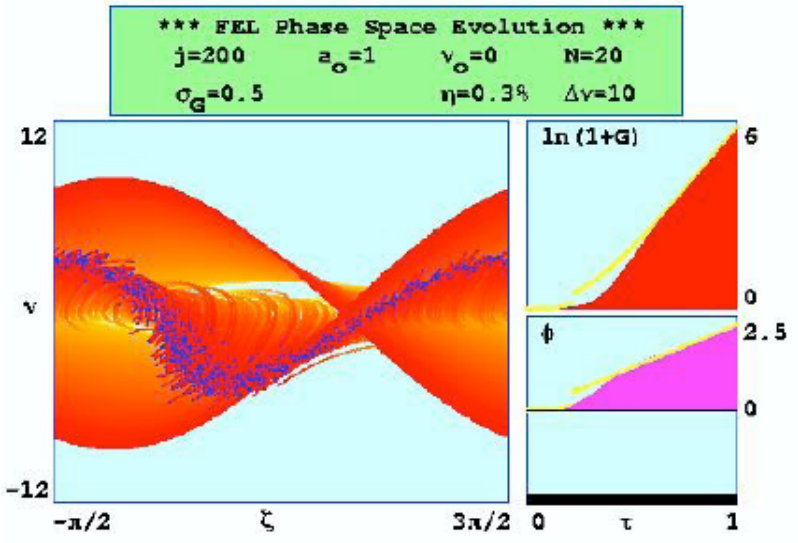

Figure 9. Phase Space of High Gain Regime ([From Ref. [4].)

The expression for gain as the electron beam goes through the undulator in the high-gain regime is given by

$$G(\tau) = \frac{1}{9} e^{(j/2)^{1/3}\sqrt{3}\tau} \text{ [7].} \qquad \text{(IV.8)}$$

The gain and phase spectra of the high-gain regime are shown in Figure 10, where the gain is almost symmetric about the resonance phase velocity. Discontinuities in the phase spectrum are due to periodic boundary conditions ($-\pi \le \phi \le \pi$).

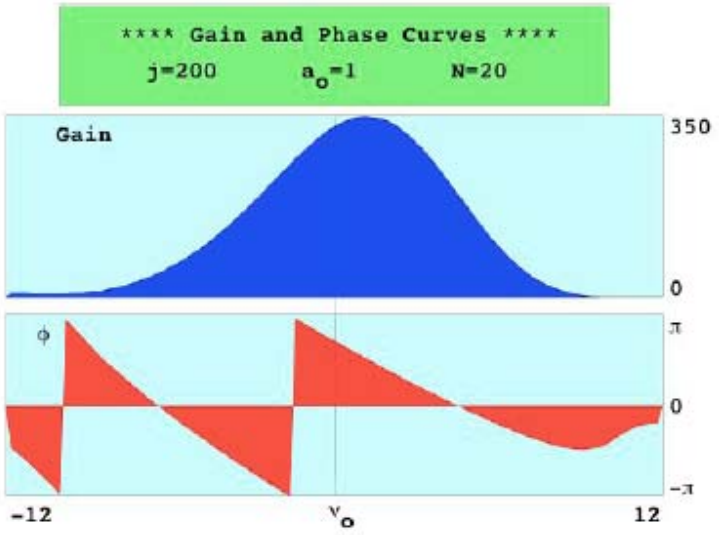

Figure 10. Gain and Phase Spectra for High Gain ([From Ref. [4].)

B. OPTICAL GUIDING

During FEL operation, the electron beam interaction opposes the normal diffraction effects of light propagation within the undulator. The optical mode is typically wider than the electron beam that interacts with it. The electrons amplify the area of the optical mode that they interact with. Therefore, the edges of the optical mode are not amplified, and as the FEL interaction continues, the central part of the mode that is interacting with the beam grows in amplitude. This interaction results in a focusing effect on the optical field in the undulator and counteracts the normal diffraction of the optical field. This is known as gain guiding. In addition, with increasing gain, there is increasing optical field phase as shown in equation IV.7. This optical field phase change counteracts the phase change that would occur due to diffraction. This is known as

optical phase guiding. Both optical phase and gain guiding benefit the FEL interaction, preventing diffraction and focusing the optical field so it overlaps the electron beam throughout the undulator. This feature allows the use of a long undulator, a vital component of a high-gain amplifier FEL.

C. BETATRON MOTION

In addition to optical guiding, there is a focusing of the electron beam itself within the undulator. In the basic theory chapter, the electrons were assumed to be perfectly injected into the undulator. In the case of imperfect injection, the electrons have variable displacements and angles from the longitudinal axis of the undulator. A displacement from the axis results in an imbalance of forces due to the undulator magnets, resulting in a low frequency sinusoidal motion known as betatron oscillation. The dimensionless betatron oscillation frequency is given by

$$\omega_\beta = \frac{2\pi NK}{\gamma} \text{ [7].} \qquad \text{(IV.9)}$$

In typical FELs, the frequency is on the order of 2π so there is about one betatron oscillation over many periods of the undulator as $\tau = 0 \to 1$. An illustration of betatron oscillation is shown in Figure 11.

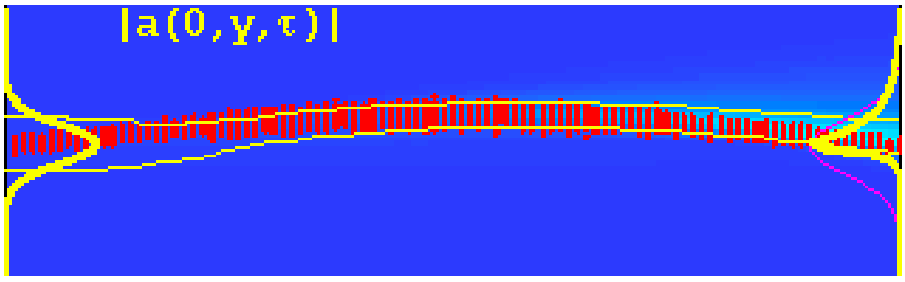

Figure 11. Betatron Focusing and Oscillation

In this figure, the electron beam (shown in red) enters at an angle that would lead to transverse beam drift along the undulator. However, the magnetic fields cause the beam to arch downwards back towards the center of the undulator. The beam's final position is slightly below the center of the undulator. If the undulator were longer, one would observe the beam bending upward back toward the center. As shown in the figure, the frequency of oscillation is low and there is typically less than one oscillation within

the undulator length. The amplitude of this oscillation for each electron depends on the beam's initial displacement and angle from the axis of the undulator. This betatron oscillation is vital in keeping the beam focused within the undulator, and allowing for imperfect electron beam injection.

D. STRONG FIELD GAIN THEORY

The initial strength of the optical field also plays an important role in the final gain of the system. In both the low and high gain regimes, a strong optical field makes the electron beam overbunch during travel through the undulator. This process is called saturation. Overbunching, as the electrons travel further through the undulator, results in energy being taken away from the optical field, reducing overall gain of the system. In the low-gain regime, saturation is achieved at much lower initial field amplitudes ($a_s \approx \pi$) than the high-gain regime ($a_s \approx 2(j/2)^{2/3}$) [7]. An example of overbunching (saturation) in the low gain regime is shown in Figure 11. When there is no saturation, the phase-space evolution of the electrons is slower and the bunch of electrons ends up in a downward trend bunched at a phase of $\zeta \approx \pi$ as shown in Figure 7. However, in this situation, the optical field is stronger, causing a greater force on the electrons and thus more evolution in phase space. The bunch forms and continues along closed orbits until it starts an upward trend, taking energy back from the optical field. This saturation can be extended, however, to achieve greater gain by tapering the undulator.

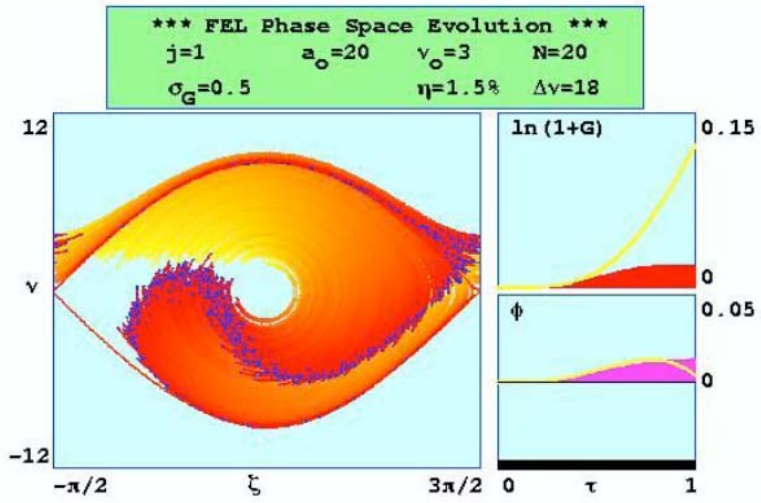

Figure 12. Low Gain Strong Field Saturation ([From Ref. [4].)

E. TAPERING

To increase extraction levels in the amplifier configuration of the FEL, some designs have utilized the concept of tapering the undulator. Tapering alters the resonance condition (equation III.22) as the electron beam travels through the undulator, allowing prolonged electron beam-optical field energy exchange. This prolonged exchange leads to higher extraction η, or percentage of energy taken from the electron beam.

Examining the resonance condition reveals that there are several ways that resonance can be affected: changing the undulator parameter, undulator period, or electron beam energy. Almost all of the tapered designs of FELs utilize the easiest of the three methods: varying the undulator parameter by changing the magnetic fields along the undulator. This is typically done by changing the separation distance (gap) between the magnets, either linearly or in a "step" change [8].

In the linear taper, a reduced (negative taper) or increased (positive taper) gap between facing magnets is introduced after the first period of the undulator. With each undulator period, the gap is either reduced or increased linearly through the rest of the undulator. The increase (or decrease) in the gap is very small (on the order of tenths of millimeters). This technique effectively exposes the electron beam to a decreasing magnetic field as shown in Figure 12 in the case of positive linear tapering, and an increasing magnetic field as shown in Figure 13 for negative linear tapering.

Figure 13. Positive Linear Tapered Undulator Field ([From Ref. [4].)

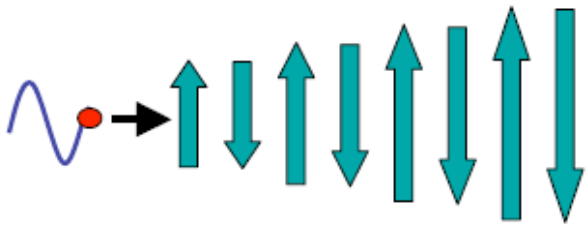

Figure 14. Negative Linear Tapered Undulator Field ([From Ref. [4].)

The step taper is implemented by changing the undulator gap at a certain point within the undulator and maintaining the reduced or increased gap through the rest of the undulator. Examples of the positive and negative step-tapered undulator are shown in Figure 14 and Figure 15.

Figure 15. Positive Step-Tapered Undulator Field ([From Ref. [9].)

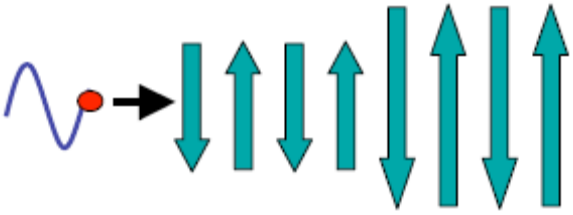

Figure 16. Negative Step-Tapered Undulator Field ([From Ref. [9].)

Tapering changes the pendulum equation to the following form,

$$\overset{\circ\circ}{\zeta} = \delta + |a|\cos(\zeta + \phi) \text{ [7]}, \qquad \text{(IV.10)}$$

$$\delta = -4\pi N \frac{K^2}{1+K^2}\frac{\Delta K}{K},$$

where δ is the phase acceleration introduced by the tapering of the undulator and $\Delta K / K$ represents the fractional change in the undulator parameter. Recall that K is proportional to B, the magnetic field strength.

This phase acceleration plays a big part in the additional extraction that a system can gain due to the tapering of the undulator. The optimum extraction from a normally configured undulator is approximately

$$\eta \approx \frac{1}{2N} \text{ [7]}, \tag{IV.11}$$

while the amount of extraction from a tapered undulator is given by

$$\eta_\delta \approx \frac{|\delta|}{8\pi N} \text{ [7]}. \tag{IV.12}$$

Equation IV.11 shows that the more taper increases, the greater the extraction levels will be; however, there is an upper limit to the amount of tapering that can be used. The upper limit is set by the fact that the pendulum equation has no solution when the taper phase acceleration is greater than the optical field amplitude. Also, a lower limit on tapering is determined by the maximum deceleration a trapped electron can undergo in the non-tapered case. This is given by doubling the separatrix height, $2|a|^{1/2}$. The two conditions set the optimal range for tapering given by

$$4\sqrt{a} < \delta < |a| \tag{IV.13}$$

In phase space, the separatrix that results from this altered pendulum equation is oriented differently depending on the type (positive or negative) of tapering. Figure 17 illustrates the phase space evolution for a positively tapered undulator, while Figure 18 depicts the results of negative tapering.

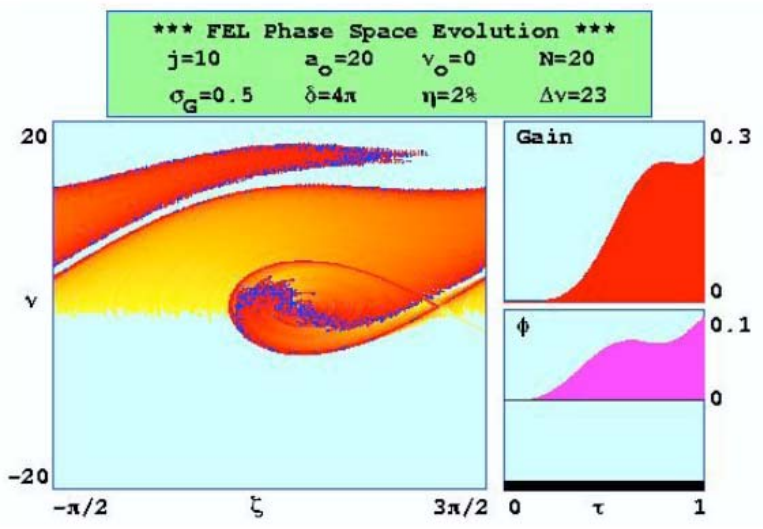

Figure 17. Positive Linear Taper Phase Space Plot (From Ref. [4].)

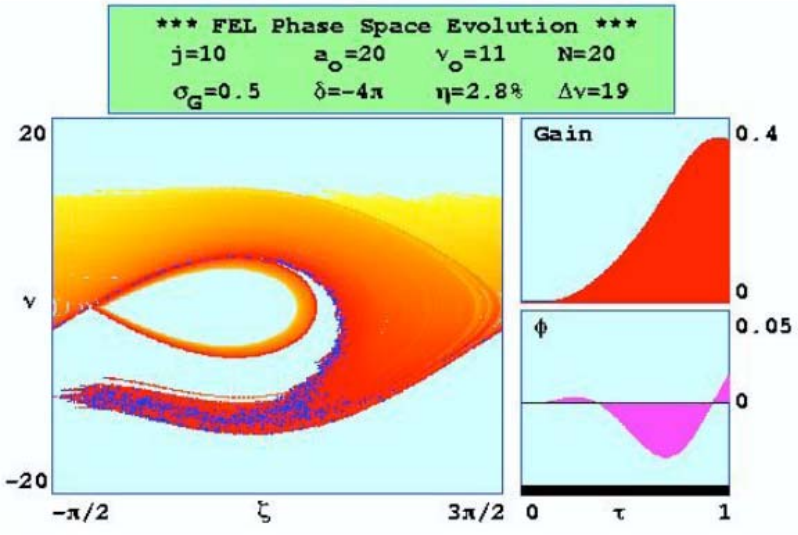

Figure 18. Negative Linear taper Phase Space Plot ([From Ref. [4].)

In the case of positive taper, some of the electrons are trapped inside the separatrix while the others are in open orbits, while in the negative tapering case, none of the electrons are trapped inside the separatrix, but must go around it. This motion around the separatrix causes bunching and good extraction. However, negative taper only works well when the electron beam starts above resonance.

The separatrix in phase space decreases in size as the phase acceleration (or deceleration) approaches the value of the optical field amplitude. When the phase

acceleration is greater, the separatrix vanishes. Without the separatrix, there are no trapped electrons and no significant bunching occurs.

Tapering, when applied optimally within the valid range, can yield significant improvement in extraction levels over a conventional FEL, especially in the high-gain and strong field regimes.

THIS PAGE INTENTIONALLY LEFT BLANK

V. BROOKHAVEN NATIONAL LAB 100-KW FEL

A. INTRODUCTION

The free electron laser shows great promise as a naval weapon, but is not yet mature enough in its design to produce the power output levels required for use in weapons application. The most powerful FEL in the world today (an oscillator configuration) is located at Jefferson Lab. It produces a continuous wave output of 10 kW, two orders of magnitude short of the MW level needed. Two competing designs for a 100 kW level FEL, proposed by Brookhaven and Los Alamos National Labs, both amplifiers, provide another vital step in the evolution of the weapons level design. This chapter will focus on the Brookhaven design, which utilizes a conventional, non-tapered undulator. The parameters of the design are shown in Table 1.

Frequency (MHz)	704	Wiggler Input Energy Spread (%)	0.02
Bunch Charge (nC)	1.4	Wiggler Period (mm)	32.5
PRF (MHz)	357	Wiggler Length (m)	3.9
Average Beam Current (A)	0.5	Number of Wiggler Periods	120
Injector Energy (MeV)	2.5	Wiggler Gap (mm)	20
Accelerating Gradient (MV/m)	20	Peak Beam Current (A)	500
Transverse rms Emittance (μm)	5.0	Extraction (%)	0.5
Longitudinal rms Emittance (keV-psec)	38	IR Output Power (kW @ 1 μm)	200
Wiggler Energy (MeV)	80	Bunch Length (psec)	2.8
Wiggler Beam Power (MW)	40	Beam Dump Power (MW)	1.25

Table 1. Brookhaven National Lab (BNL) Design Parameters ([After Ref. [10].)

B. PERFORMANCE OF THE BROOKHAVEN FEL DESIGN

Computer simulations using codes developed at the Naval Postgraduate School were run to determine the performance of the design with the electron beam misaligned in various ways.

1. Weak-Field Gain Spectrum

The Brookhaven FEL design was first simulated with an aligned electron beam injection to study its gain and extraction spectrum. To obtain the gain spectrum, the electron beam phase velocity ν_0 (proportional to energy) was varied and the optical field kept in the weak field regime ($a_0 \ll (j/2)^{2/3}$). The gain spectrum is shown in Figure 19.

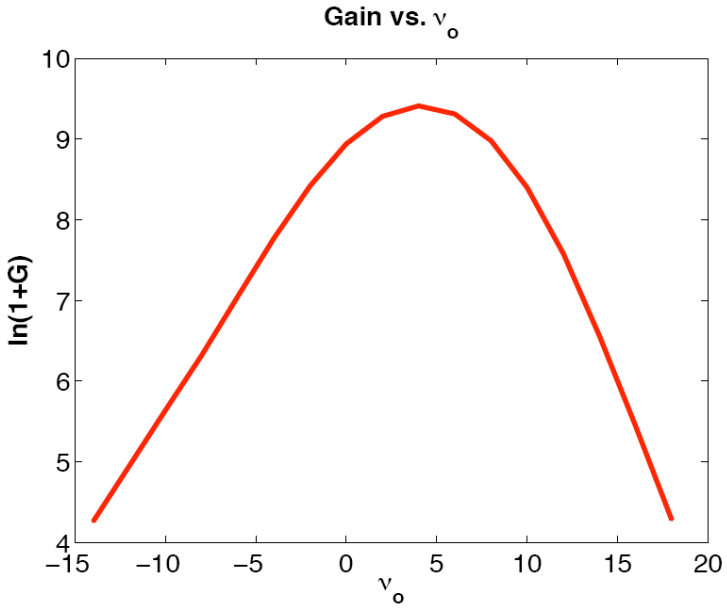

Figure 19. BNL FEL Weak-Field Gain Spectrum

Examining the gain spectrum, one sees the broad spectrum indicative of a high gain FEL, with a maximum of G ~12000 at $\nu_0 = 4$. This phase velocity corresponds to a optical wavelength shift of 0.5% above resonance. The effects of high gain optical guiding can be examined at the peak of the gain spectrum. A picture of the interacting electron beam (shown in red) and optical field (shown in yellow) within the undulator is shown in Figure 20.

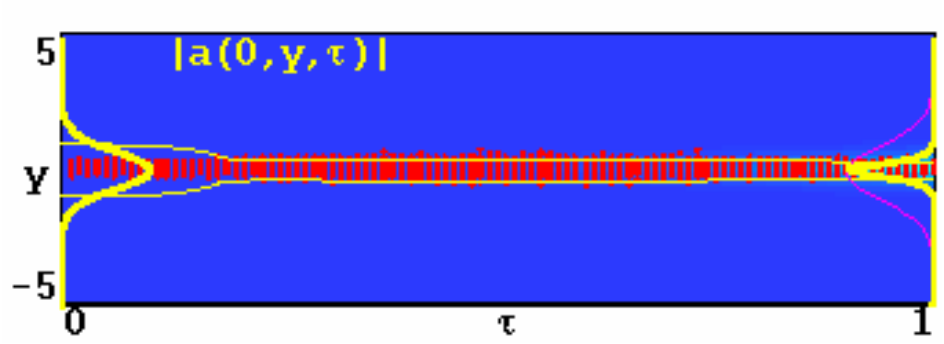

Figure 20. Simulation of Gain Guiding at Peak Gain of BNL Design

At the beginning of the undulator, where gain is low, the initial optical mode is fairly wide. As the optical mode proceeds through the undulator and interacts with the electron beam, gain guiding amplifies the central part of the mode and counteracts the phase change due to diffraction, focusing the mode in the center of the undulator. The resulting amplified mode is significantly narrower at the end of the undulator. This reduced the optical mode size, so that it will diffract to a larger area at the first subsequent optic, resulting in a smaller intensity on the optic. The minimization of intensity on optics is an important issue in the design of any high-power FEL.

2. Extraction Spectrum

Simulations at various initial electron beam phase velocities ν_0 determined the maximum extraction η, defined as the output laser power divided by the power in the electron beam entering the undulator. The simulations result in the extraction spectrum of Figure 21.

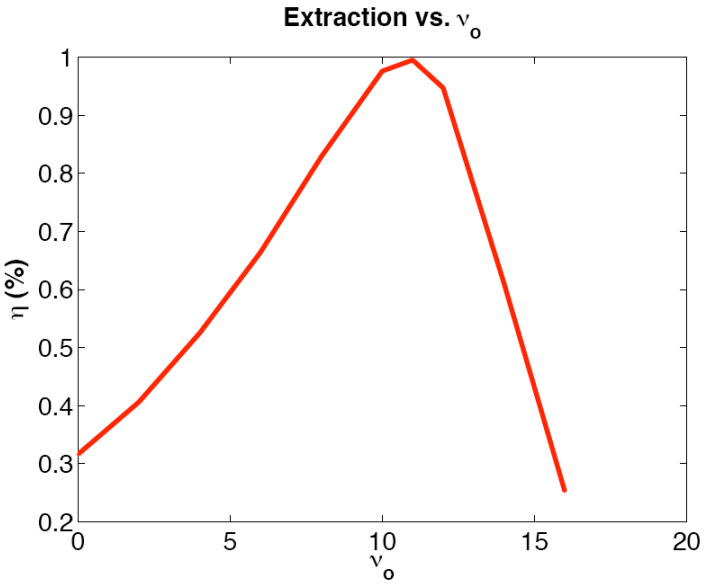

Figure 21. Brookhaven FEL Extraction Spectrum

The maximum extraction that this design will achieve is approximately one percent. This maximum occurs at an electron beam initial phase velocity of $\nu_0 = 11$, corresponding to a wavelength shift of 1.5% away from resonance. With an electron beam power of 40 MW, this extraction yields an output power of 400 kW, which is four times the design specification of the FEL. A minimum extraction of only 0.25% is required to yield the design specified 100 kW output power.

From the optimal extraction simulation, the electron beam-optical field interaction yields the phase space picture of Figure 22, where there is an induced electron beam energy spread of 4%. The vertical axis is proportional to the electron energy while the horizontal axis is the electron phase within an optical wavelength.

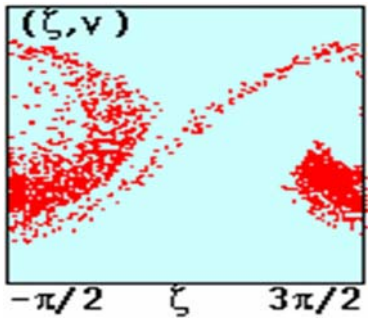

Figure 22. BNL FEL Optimal Phase Space

Gain is not optimal when extraction is maximized, but the FEL still reaps the benefits of gain guiding as shown in Figure 23. The Gaussian shape in red at the right end of the undulator represents the optical mode size due to normal free space diffraction. The yellow is the actual mode. There is seen to be significant focusing due to the electron beam interaction.

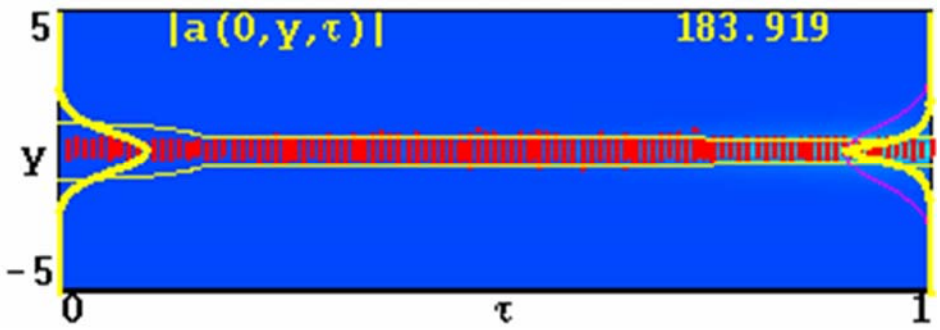

Figure 23. Gain Guiding in Optimal Extraction Simulation of BNL FEL.

Optical guiding in the undulator leads to increased diffraction and a bigger mode radius at the first optic as shown in Figure 24. The theoretical optical mode size due to diffraction is shown in red, while the actual mode (approximately twice the size) is shown in yellow.

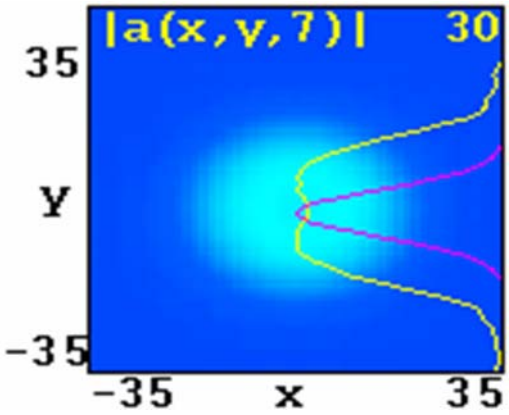

Figure 24. Optical Mode at First Optic (27 m away)

The spot area on the first optic spaced at 27 meters from the beginning of the undulator is approximately 12 cm^2 so the resulting intensity at the first optic is 30

kW/cm^2. The x and y axes in Figure 24 refer to the transverse extent of the optical mode intensity shown by the brighter area in the background of the figure.

3. Electron Beam Shift

Vibration tolerances of the Brookhaven FEL design are analyzed in the next two sections. Onboard ship, vibrations affecting the FEL have an extremely low frequency when compared to the pulse repetition frequency of the optical beam in the undulator. For this reason, vibration effects (shift and/or tilt of the electron beam) can be modeled as static conditions in the Brookhaven FEL.

Vibration, in essence, results in imperfect electron beam injection into the undulator. The case of a vertical transverse shift of the electron beam away from the undulator axis is studied first. Many simulations optimize the extraction in ν_0 at various amounts of electron beam shift off the undulator axis, producing the results shown in Figure 25.

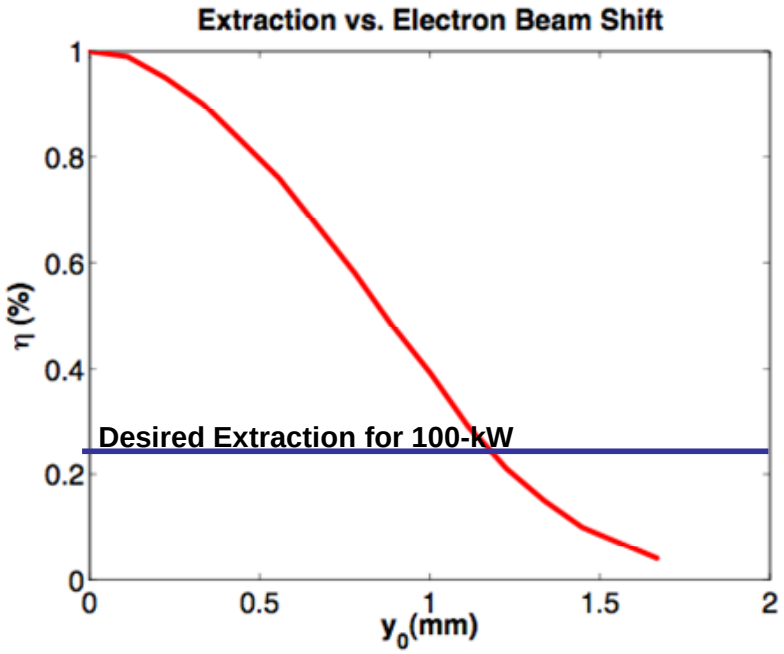

Figure 25. Extraction vs. Electron Beam Shift

As expected, performance of the system is degraded and extraction decreases as the electron beam shift increases. A maximum tolerable shift of approximately 1.2 mm

would still allow the FEL to produce the specified output power of 100 kW. Figure 26 shows the effect of a large electron beam shift in the undulator.

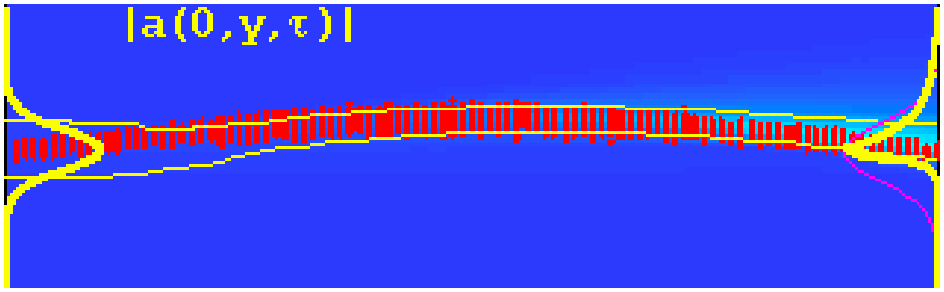

Figure 26. Electron Beam Shift in the Undulator

Betatron focusing deflects the electron beam back to the center of the undulator. There is also optical guiding as the beam bends in the undulator. These effects, unfortunately, result in a distorted, non-symmetric optical mode exiting the undulator. Experimental FEL systems with active alignment can hold the electron beam displacement y_0 to within 0.05 mm, so there is expected to be only a small amount of degradation due to vibration.

4. Electron Beam Tilt

The Brookhaven FEL design is also subjected to another effect of vibration: the electron beam entering the undulator an angle. Simulations were run (and optimized with respect to ν_0) for varying angles to determine the effect of the angle of the electron beam at the middle of the undulator on extraction. The resulting graph is shown in Figure 27. Each value of extraction is evaluated at the optimum ν_0.

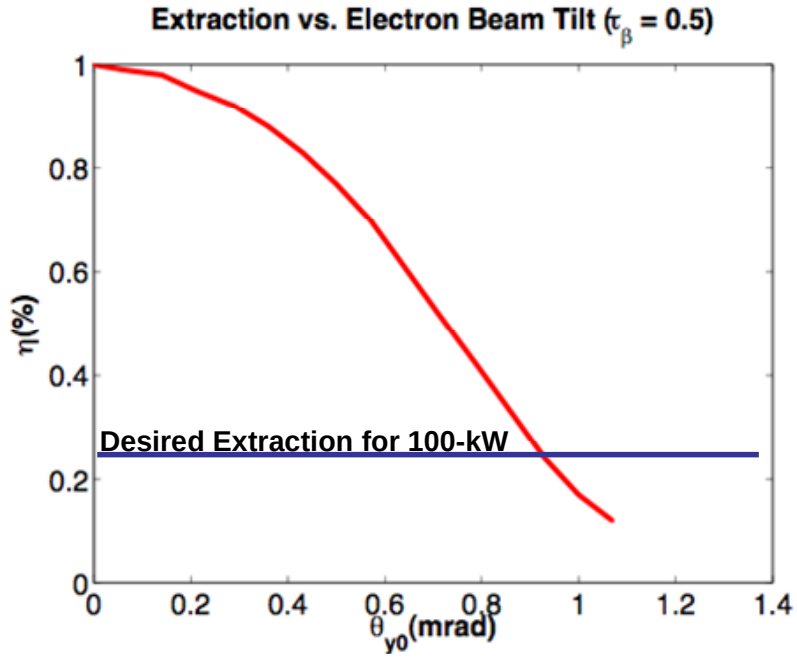

Figure 27. Extraction vs. Electron Beam Tilt at Middle of Undulator

The performance of the system is hampered by the angle of the electron beam, as shown by the decreasing extraction with increasing angle of tilt. Performance is degraded most severely (i.e. steeper slope) with shifts of approximately 0.6 mrad or greater. A maximum electron beam tilt of approximately 0.9 mrad still allows the system to produce designated output power. A simulation at the maximum allowable tilt (Figure 28) illustrates this effect with electron beam focusing at the midway point of the undulator.

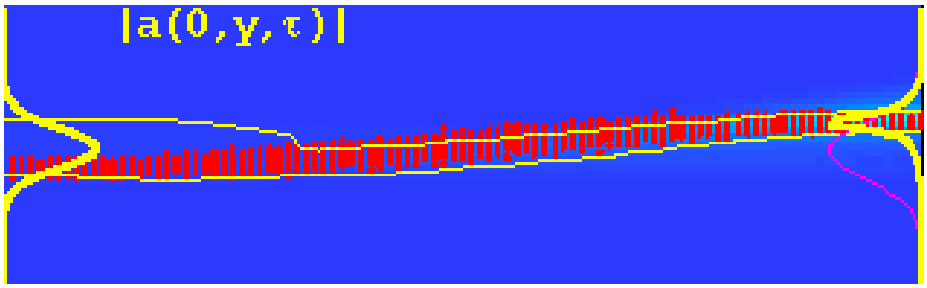

Figure 28. Electron Beam Tilt Midway Through Undulator

Betatron motion keeps the electron beam focused enough in the undulator, but the output optical mode is shifted vertically upon exiting the undulator due to optical guiding

by the angled electron beam. These effects result in a poorly shaped optical mode at the first optic. An experimental FEL system with active alignment is expected to have an angular tolerance of 10 μrad, so that only a very small amount of degradation is actually anticipated.

The same procedure is then performed with the electron beam angled upon entry into the undulator. The result of these simulations is shown in Figure 23, with extraction at each point optimized in ν_0.

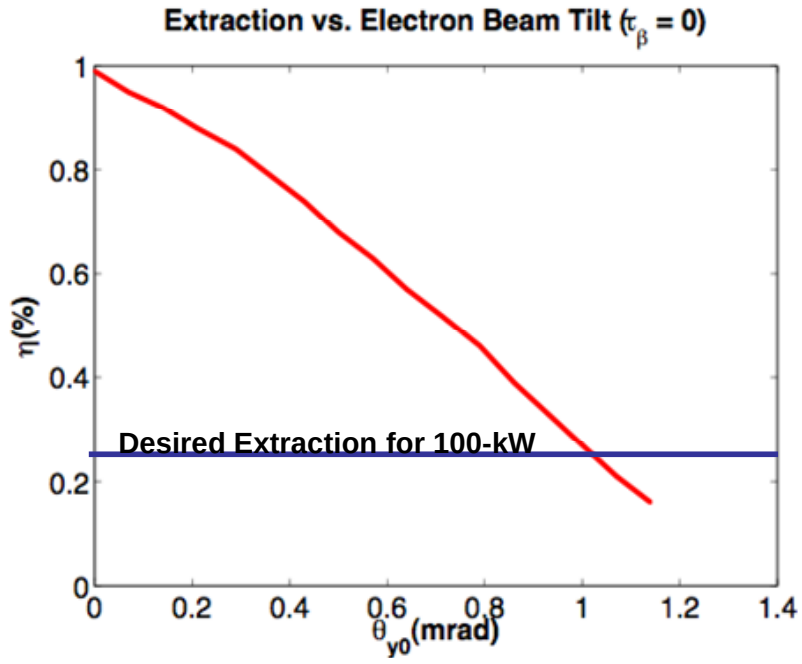

Figure 29. Extraction vs. Beam Tilt at Beginning of Undulator

As seen in the prior case, increasing the angle degrades performance, but the decrease in extraction is nearly linear. In addition, the tolerance of electron beam tilt is increased to approximately 1 mrad. Figure 30 illustrates the effect of tilt with electron beam focus at the beginning of the undulator.

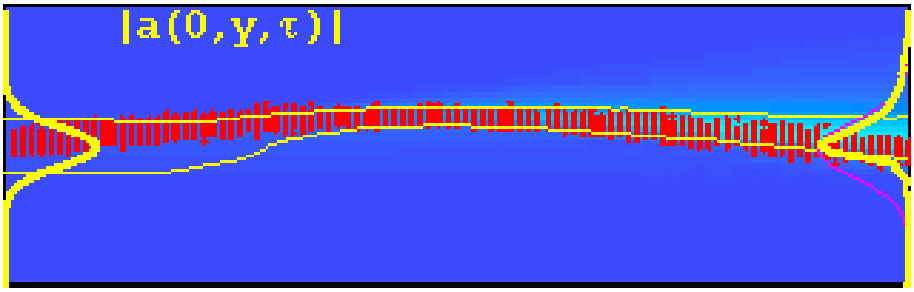

Figure 30. Electron Beam Tilt at Beginning of Undulator

With focusing at the beginning of the undulator, betatron focusing works better and the mode is not shifted, and is nearly symmetric. This results in a useable optical mode at the first optic. But, again, with active alignment, such large angular deflection would not occur.

In the case of all vibration effects studied, experiments running today are able, through active alignment, to keep well within the thresholds, making vibration a non-issue to the Brookhaven FEL.

VI. LOS ALAMOS NATIONAL LAB 100 KW FEL

A. INTRODUCTION

Another design for a 100 kW FEL has been proposed by Los Alamos National Lab (LANL). The parameters for the design are listed in Table 3 below. Non-tapered and linearly tapered variants of this design are analyzed in this chapter.

Beam Energy	80.8 MeV	Matched Beam Radius	0.27 mm
Peak Current	1 kA	Beam Radius at Wiggler Entrance	0.11 mm
Rms Emittance	10 mm-mrad	LANL Extraction	1.9%
rms Energy Spread	0.25	Wiggler Length	2.4 m
Wiggler Period	2.18 cm	Wiggler Parameter	1.2

Table 2. Los Alamos National Lab Design Parameters ([After Ref. [8].)

B. NON-TAPERED DESIGN PERFORMANCE

1. Extraction Spectrum

As a basis for comparison, a non-tapered version of the Los Alamos design is simulated and its performance optimized. These simulations result in the extraction spectrum shown in Figure 31.

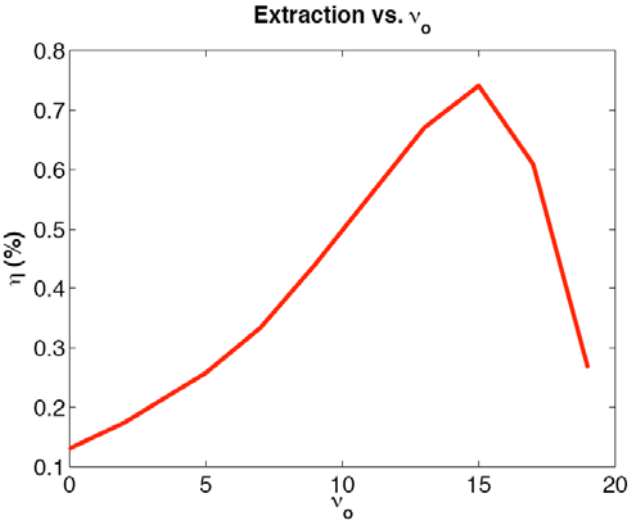

Figure 31. LANL Non-Tapered Extraction Spectrum

The extraction spectrum peaks at ($\nu_0 = 15$), corresponding to a wavelength shift of 2.1% away from resonance. The maximum extraction obtained by this design is approximately 0.75%, producing an output power of 60 kW from the 8 MW electron beam. This output fails to meet design specifications, showing that tapering is needed to boost performance of the design.

C. LINEAR TAPERED DESIGN PERFORMANCE

1. Weak-Field Gain Spectrum

An alternate design was explored using a linear taper. Several simulations were run to optimize the amount of taper and the position in the undulator where the taper begins. For the optimized design, the taper begins at a point 60% of the way down the undulator length with a maximum change $\Delta B / B$ of 18% in the undulator magnetic field. This design was then analyzed for performance and to determine vibration tolerances. The weak field gain spectrum is shown in Figure 32.

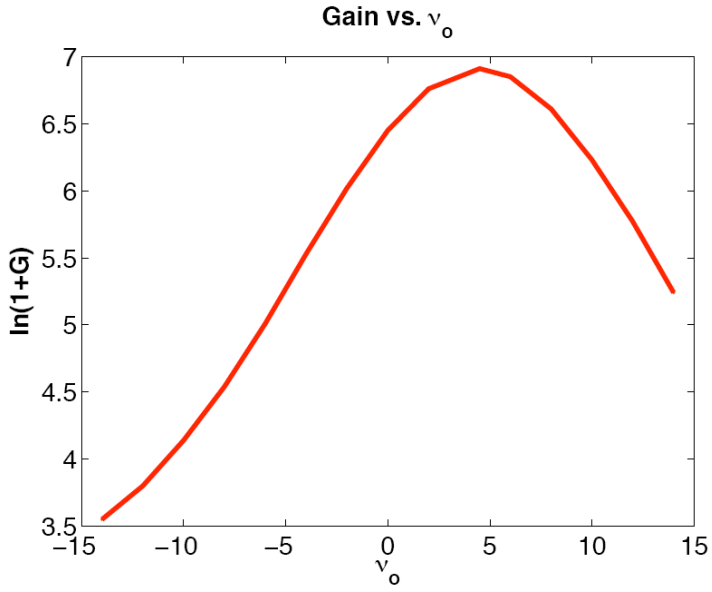

Figure 32. LANL Linear Tapered FEL Weak-Field Gain Spectrum

The gain spectrum is very broad in ν_0 with maximum gain of approximately 900 occurring at ($\nu_0 = 4.5$), corresponding to a wavelength shift of 0.65% away from resonance ($\nu_0 = 0$).

2. Extraction Spectrum

The design is simulated and optimized to determine the maximum extraction. The extraction spectrum is shown in Figure 33.

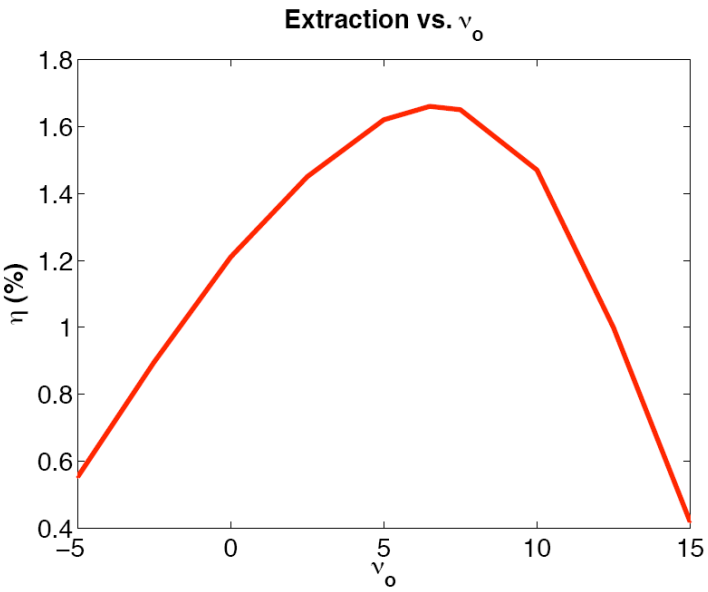

Figure 33. LANL Linear Tapered FEL Extraction Spectrum

With a minimum extraction of 1.2% required for an output of 100 kW, this design's extraction spectrum peaks at ($\nu_0 = 6.5$), corresponding to a wavelength shift of 0.94% away from resonance. The maximum extraction is found to be 1.66%, resulting in an output power of 133 kW. This power level is more than double that of the non-tapered design, showing the benefits of a tapered undulator.

Figure 34 shows that this design, when operating at optimum, benefits from optical guiding, resulting in a smaller optical mode waist centered at the end of the undulator.

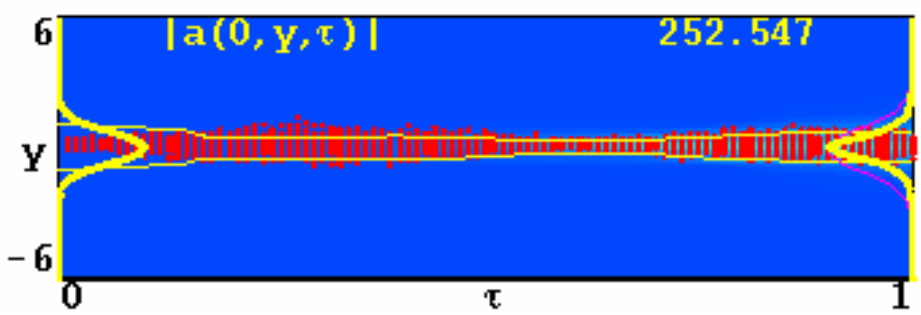

Figure 34. Optical Guidance in a Linear Tapered LANL FEL Design

As a benefit of optical guiding, the output laser beam diffracts to a larger size in free space after the interaction in the undulator, resulting in a larger mode waist at the first optic and lower intensity. The mode waist is approximately 2.2 cm at the first optic 24 meters away, and the resulting intensity is approximately 9 kW/cm^2. The resulting laser mode at the first optic is pictured in Figure 35.

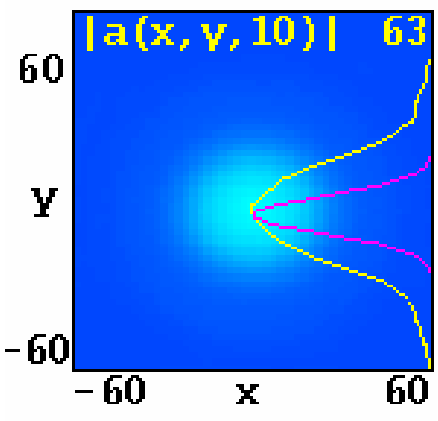

Figure 35. Optical Mode at the First Optical Element (24 m)

This low intensity level poses no problems for the mirrors used in FEL systems currently in operation which are able to handle intensities of 100 kW/cm^2 for extended periods of time.

The phase space plot shown in Figure 36 differs from the Brookhaven design (Figure 22) with approximately half of the electrons trapped and half free. The tapered undulator creates an increased induced energy spread of approximately 6%.

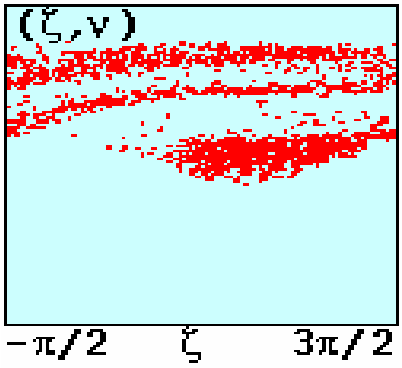

Figure 36. Phase Space Plot of Linear Tapered LANL Design

3. Electron Beam Shift

The linear-taper design was simulated under varying conditions of electron beam shift and tilt. The result of several simulations with varying amounts of electron beam shift y_0 is shown below in Figure 37.

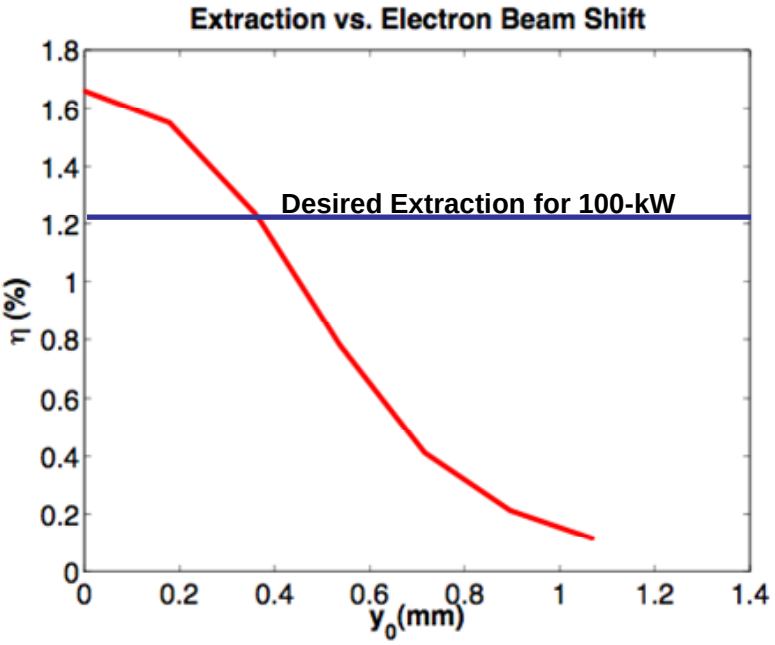

Figure 37. LANL Linear Tapered FEL Extraction vs. Electron Beam Shift

The LANL design must extract 1.2% of the electron beam energy to achieve the rated power output of 100 kW. Examining the figure, this is accomplished with an electron beam shift of up to approximately 0.4 mm, a shift equal to four times the radius

of the electron beam. A simulation with the maximum tolerable electron beam shift shown in Figure 38 illustrates the effects in the undulator.

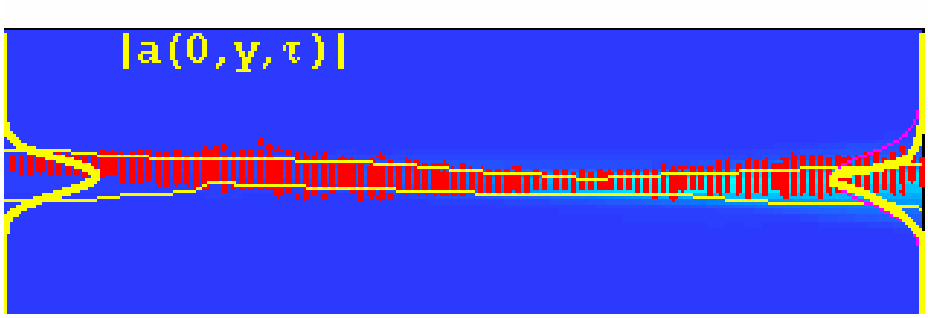

Figure 38. Maximum Electron Beam Shift on Linear Tapered LANL FEL

Betatron focusing and optical guiding allows the FEL to produce rated output, but the laser output mode is slightly distorted upon exiting the undulator.

4. Electron Beam Tilt

The linearly tapered design was simulated with varying degrees of electron beam tilt and focus. The result of the simulations is plotted in Figure 39.

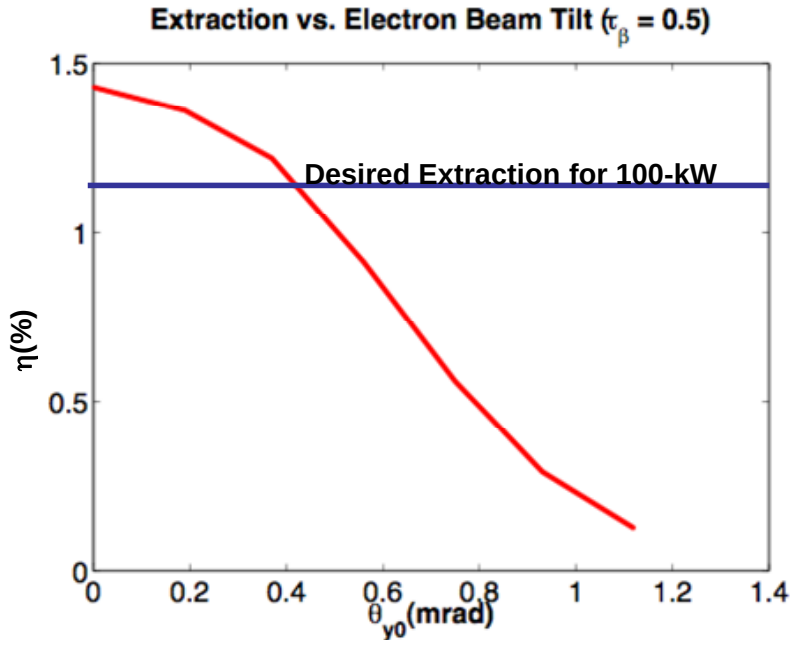

Figure 39. LANL Extraction vs. Electron Beam Tilt at Middle of Undulator

A maximum tilt of approximately 0.5 mrad at the middle of the undulator is allowed before the FEL fails to produce the designed power output. Figure 40 illustrates the electron beam interaction with the optical field in the undulator.

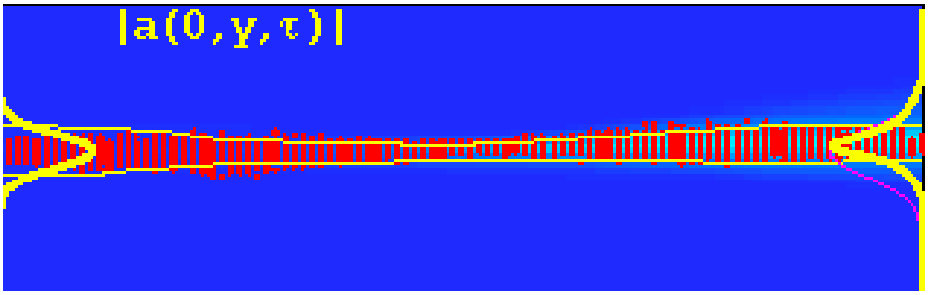

Figure 40. Maximum Electron Beam Tilt at Middle of Undulator

Betatron focusing and optical guiding results in a smaller symmetric, but slightly shifted output laser optical mode exiting the undulator.

Simulations were repeated with the electron beam tilted at the beginning of the undulator, resulting in Figure 41.

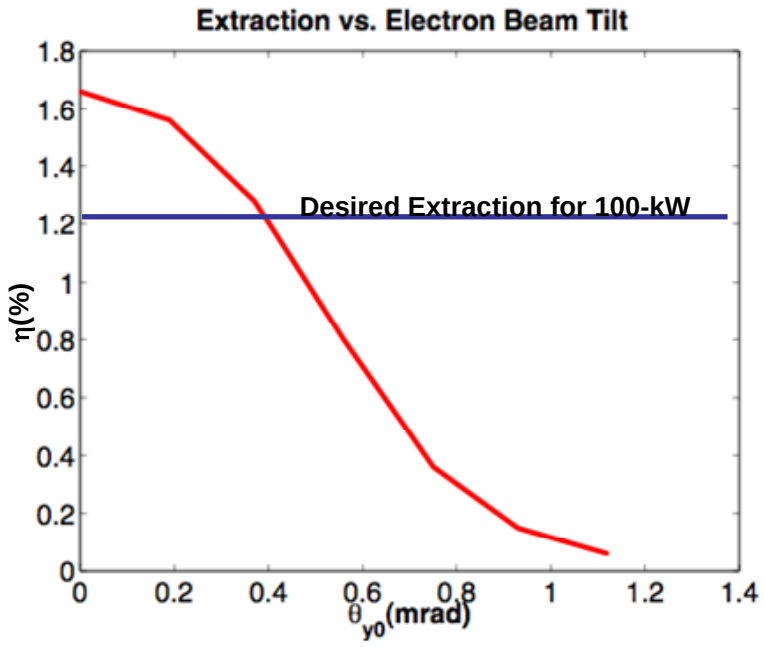

Figure 41. LANL FEL Extraction vs. Beam Tilt at Start of Undulator

With the electron beam tilted at the beginning of the undulator, there is a decrease in tolerance of electron beam angle, with a maximum tolerable tilt of 0.4 mrad for design output power. A simulation snapshot of the extreme limit shown in Figure 42 illustrates the effect of the electron beam tilt on the optical output of the undulator.

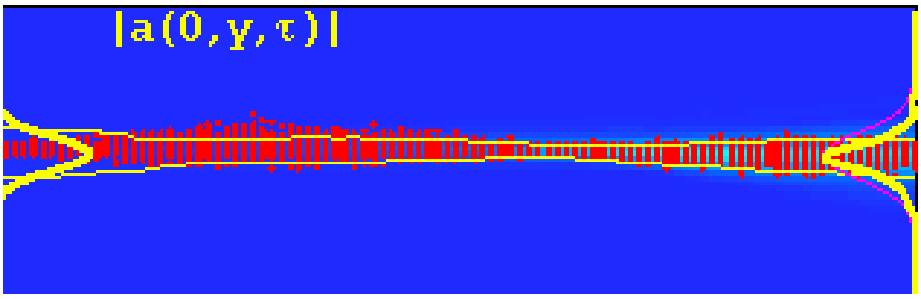

Figure 42. Electron Beam Tilt at the Beginning of the Undulator

In this case, the effects of the tilt are not as apparent in the undulator. Betatron focusing keeps the electron beam fairly straight within the undulator. The optical guiding results in the optical mode centered in the undulator and only slightly distorted.

As with the case with the Brookhaven design, the Los Alamos design can tolerate vibrations such that the electron beam, through active alignment, will not be shifted or tilted enough to hamper performance.

5. Variation of Electron Beam Focus

In examining the two cases of electron beam tilt at different locations along the undulator, there were higher extraction levels where the electron beam was tilted at the beginning of the undulator. This section examines the correlation between system performance and electron beam focus points within the undulator. Simulations are run with perfect electron beam injection, varying the electron beam focus point within the undulator. The summary of results is plotted in Figure 30.

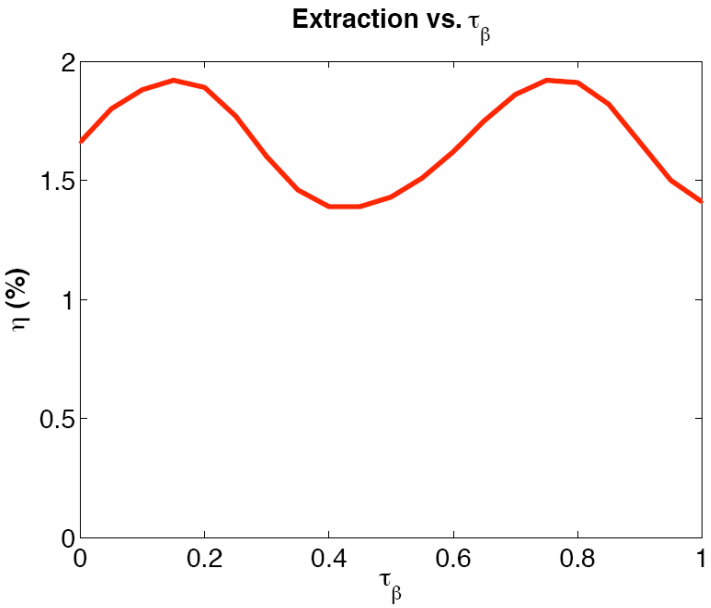

Figure 43. LANL Extraction versus Electron Beam Focus Point

The extraction of the FEL is roughly sinusoidal with the position of electron beam focus within the undulator, with peak extraction of 1.9% at $\tau_\beta = 0.15$ and $\tau_\beta = 0.75$ down the length of the undulator. At this new focus the output is 153 kW, a 20 kW improvement over the baseline design.

THIS PAGE INTENTIONALLY LEFT BLANK

VII. CONCLUSION

We have examined both the Brookhaven and Los Alamos designs, and have determined that the Brookhaven design can produce a higher output, namely 400 kW. The BNL design did not allow for a tapered undulator due to limits in acceptable electron beam energy spread required for recirculation. With an increase in electron beam energy and average current, this design could achieve an output of the desired megawatt level.

We have also compared the non-tapered and linear-tapered versions of the Los Alamos design, and find that the tapered version has more than twice the extraction, demonstrating the benefits of a tapered undulator. The linearly tapered design was able to produce an output of 153 kW, while the non-tapered managed only 60 kW. As with the Brookhaven design, with increased electron beam energy and average current, the tapered design is capable of producing a megawatt level laser beam.

Vibration effects of electron beam shift and tilt were, for the first time, studied for the amplifier configuration of the FEL. Results for both the Brookhaven and Los Alamos designs prove promising, with experiments currently in operation able to hold electron beam tolerances for both shift and tilt to within an order of magnitude less than the physical tolerances of the designs in achieving rated output. The designs, when simulated with shift and tilt on the order of the experimental tolerances, had negligible performance degradation.

Future work in this area includes further analysis of the Brookhaven FEL to minimize the energy spread induced in the electron beam during operation while maintaining the designed output level. There is an alternate 100 kW FEL operates at Brookhaven National Lab which could be studied by us once we receive the physical parameters of the design.

The actual design proposed by Los Alamos National Lab was a step-tapered undulator. This design could be studied more closely for optimization and tolerance effects similar to those performed for this thesis.

Once a design is agreed upon that will yield the power necessary for a possible weapon system, there are several issues that must be addressed for using the FEL onboard a ship. These include beam transport, optical element damage (namely the first optical element), and propagation of the high energy laser through the atmosphere to the target.

LIST OF REFERENCES

1. Thornton, Stephen T. and Andrew Rex, *Modern Physics for Scientists and Engineers*, p.320, Jefferson City: Thompson Learning Inc., 2002.

2. Committee on Free Electron Lasers and Other Advanced Coherent Light Sources, *Free Electron Lasers and Other Advanced Sources of Light: Scientific Research Opportunities*, p.16, Washington D. C.: National Academy Press, 1994.

3. Williams, Gwen, "Specifications of the Jlab FEL," [http://www.jlab.org/FEL/felspecs.html]. February 2005. 17 April 2006.

4. O'Shea, Patrick, Joe Blau, Bill Colson, Steve Benson, George Neil, and Dinh Nguyen, *DEPS Free Electron Laser Short Course*. pp 25-50, Albuquerque: DEPS, 2003.

5. Barish, Barry, "Technology Breakthroughs and International Linear Collider," Presentation, AAAS Conference, Washington D. C., February 2005.

6. "Undulator." *Wikipedia, The Free Encyclopedia*, [http://en.wikipedia.org/wiki/Undulator]. 10 March 2006. 17 April 2006.

7. Colson, W. B., C. Pellegrini, and A. Renieri, eds., *Free Electron Laser Handbook*. The Netherlands: Elsevier Science Publishing Co. Inc., 1990.

8. Nguyen, D. C., H. P. Fruend, and W. B. Colson, "High-power free-electron laser amplifier using a scalloped electron beam and a two-stage wiggler." Physical Review Special Topics – Accelerators and Beams, pp.1-3, (2006).

9. William B. Colson, Class Notes, PH 4858 – Electric Ship Weapon Systems, Winter 2006.

10. Ben-Zvi, Ilan. "A 100 kW FEL Risk Reduction Program," Presentation, FEL Working Group, Newport News, VA May 2005.

THIS PAGE INTENTIONALLY LEFT BLANK

INITIAL DISTRIBUTION LIST

1. Defense Technical Information Center
   Ft. Belvoir, Virginia

2. Dudley Knox Library
   Naval Postgraduate School
   Monterey, California

3. Robert F. Walter
   Schafer Corporation
   Albuquerque, NM

4. CAPT (Ret) Roger McGinnis
   Office of Naval Research
   Arlington, VA

5. Quentin Saulter
   Office of Naval Research
   Arlington, VA

6. Dr. Alan Todd
   Advanced Energy Systems, Inc.
   Princeton, NJ

7. Dr. Fred Dylla
   Thomas Jefferson National Accelerator Facility
   Newport News, VA

8. Dr. George Neil
   Thomas Jefferson National Accelerator Facility
   Newport News, VA

9. Chairman, Physics Department
   Naval Postgraduate School
   Monterey, CA

10. Professor William B. Colson
    Naval Postgraduate School
    Monterey, CA

11. Dr. Starnes Walker
    Office of Naval Research
    Arlington, VA

12. Dr. Ilan Ben-Zvi
Brookhaven National Lab
Long Island, NY

13. Dr. Dinh Nguyen
Los Alamos National Lab
Albuquerque, NM